NUREG/CR-1825
ANL-79-10

Distribution
Code: R7

ARGONNE NATIONAL LABORATORY
9700 South Cass Avenue
Argonne, Illinois 60439

AN OVERVIEW OF ROD-BUNDLE THERMAL-HYDRAULIC ANALYSIS

by

William T. Sha

Components Technology Division

November 1980

Prepared for

Office of Nuclear Regulatory Research
U. S. Nuclear Regulatory Commission
Washington, D. C. 20555
under Interagency Agreement DOE 40-550-75

NRC FIN No. A2045

AN OVERVIEW ON
ROD-BUNDLE THERMAL-HYDRAULIC ANALYSIS

by

William T. Sha

ABSTRACT

Three methods used in rod-bundle thermal-hydraulic analysis are summarized. These methods are: (1) subchannel analysis, and its inherent assumptions are clearly stated; (2) porous medium formulation with volume porosity, surface permeability, distributed resistance and distributed heat source (sink) - the concept of surface permeability is new in porous medium formulation, and greatly facilitates modeling anisotropic effects; and, (3) benchmark rod-bundle thermal-hydraulic analysis using a boundary-fitted coordinate system, and it represents the most rigorous method to date. For laminar flow, this method gives solutions without any assumptions and it requires information on rod bundle geometry and thermal physical properites of the fluid. Basic limitations and merits of each method are discussed in detail.

NRC FIN No. | Title

A2045 | 3-D Time-dependent Code Development

TABLE OF CONTENTS

TABLE OF CONTENTS (CONTD.)

LIST OF FIGURES

LIST OF TABLES

EXECUTIVE SUMMARY

Three pertinent methods used in rod-bundle thermal-hydraulic analysis are presented. These methods are (1) subchannel analysis, (2) porous medium formulation, and, (3) benchmark rod-bundle thermal-hydraulic analysis using a boundary fitted coordinate system. Basic limitations and merits of each method are delineated.

The subchannel method is the most widely used in rod-bundle thermal-hydraulic analysis to date. Historically, and as originally intended, subchannel analysis has been used primarily for design calculations. It explicitly assumes that one of the velocity components (axial velocity) is dominant, compared to components in the other directions (crossflow velocities). Until recently, the subchannel method has been extended to reactor safety analysis, such as the resolution of flow blockage in a fuel assembly. In this case, the usus l assumptions for small crossflows in transverse directions are no longer valid. It is important to recognize that the basic limitations of a method and a computer code can only be as good as its formulation. The basic limitations of subchannel analysis are:

(1) The fine structure of both velocity and temperature within a subchannel is ignored (lumped parameter approach).

(2) The transverse momentum equations cannot be treated with the same rigor as the axial momentum equation because of non-orthogonal characteristics of subchannel arrangment. Specifically, the finite difference representation of the second derivatives cannot be rigorously evaluated.

(3) To facilitate calculations, approximations are necessary for simplifying the geometric configuration of the control volumes used in the transverse momentum equations and interfacing the required information at the various locations between control volumes for the axial and transverse momentum equations.

The above limitations are inherent; therefore, the validity of subchannel analysis to situations with large flow disturbance, such as blockage, poses concern.

The porous medium formulation with volume porosity, surface permeability, distributed resistance and distributed heat source was first proposed for rod-bundle thermal hydraulic analysis, and it eliminates some of the limitations employed in subchannel analysis. The detailed derivation via local volume averaging is presented. The concept of surface permeability is new in porous medium formulation, and it greatly facilitates characterization of an anisotropic medium. Also, it generally improves the accuracy of results since surface permeability is well defined and distributed resistance is not precisely known in most engineering applications. Furthermore, the porous medium formulation provides a greater range of applicability; it is capable of treating both continuum (reactor plenum mixing, piping analysis, etc.), and quasi-continuum (fuel assembly, heat exchanger, etc.) problems. This capability represents a very cost effective way of developing a computer code. It should be noted that since local volume averaging is used in the porous medium

formulation, high resolution of the local velocity and temperature is somewhat lost. Furthermore, just as the friction factor must be calibrated in subchannel analysis, so must the distributed resistance be calibrated with experimental data in the porous medium formulation.

The most rigorous rod-bundle thermal-hydraulic analysis is to use boundary fitted coordinate transformation. Each rod is explicitly represented as an internal boundary; thus, appropriate boundary conditions can be specified. After the coordinate transformation, the complex rod-bundle geometry reduces to a multiply connected continuum in a rectangular region with all boundaries coincident with the grid lines. However, the system of equations to be solved in the transformed plane is more complicated than the original one. Most important of all, the empirical mixing coefficients and cross flow resistances normally associated with a rod-bundle thermal-hydraulic analysis are eliminated, thereby enhancing computational stability and accuracy. As a matter of fact, for laminar flow, this method gives solutions without any assumptions, and it requires information only on rod bundle geometry and thermal physical properties of the fluid; for turbulent flow, empiricism is needed due to the enclosure problem encountered in turbulence modeling. One drawback of benchmark rod-bundle thermal-hydraulic analysis using a boundary fitted coordinate system is that it requires large computer storage and long running time, and thus,is limited to relatively small rod-bundle sizes or a local region of interest in a large rod bundle.

I INTRODUCTION

Most heat exchangers and reactor fuel assemblies employed in the power industry are in the form of rod-bundle geometry. Fluid flow and heat transfer in a rod bundle are complex phenomena, and the basic understanding of these phenomena is essential to achieving optimum design performance during normal operating conditions and maintaining structural integrity during off-normal operations.

The traditional way of obtaining detailed performance information is to build a scaled model of the heat exchanger or the reactor fuel assembly under consideration. Both heat-giving and heat-receiving fluids are then circulated through the shell and tube sides (or tube and shell sides), respectively, of the heat exchanger, or heat-receiving fluid is force-convected through the reactor fuel assembly so that both velocity and temperature measurements can be made over the expected range of operating conditions. Based on these measurements, correlations of heat transfer coefficients and pressure drops as functions of Reynolds number, geometry, etc., are developed, and subsequently, these correlations are used for designing the apparatus. This approach, however, suffers from several drawbacks: for each new geometry considered, a new test model must be constructed; scaling from the test model to design size often poses some concern. Furthermore, considerations of expenses, instrumentation and measuring technique usually limit data to global heat transfer and flow rates, while detailed temperature and velocity distributions are needed for an optimum design. Finally, correlations developed based on these measurements are valid only in the range of parameters tested; additional experimental measurements are often required when the operating conditions fall outside the range of these correlations.

An alternative approach is to develop direct numerical solutions of the conservation equations of mass, momentum, and energy, using appropriate initial and boundary conditions of the physical system under consideration. However, a major obstacle to the use of numerical methods in rod-bundle thermal-hydraulic analysis has been the complex geometry. Recently, this obstacle has been overcome by using the boundary fitted coordinate transformation. Moreover, with the anticipated improved performance of the next generation of computers and further advances in numerical solution technique, the detailed numerical simulation of rod-bundle thermal-hydraulic behavior appears practical and attractive. Accordingly, the objectives of the paper are: (1) to summarize pertinent methods employed in rod-bundle thermal-hydraulic analysis; and, (2) to delineate basic limitations and merits of each method.

II. METHODS USED IN ROD-BUNDLE THERMAL-HYDRAULIC ANALYSIS

The rod-bundle thermal-hydraulic analysis discussed in this report is limited to solution methods for conservation of mass, momentum, and energy equations considered as an initial-value problem in time, and a boundary-value problem in space; and also is limited to descriptions and performance of pertinent computer codes available in the open literature. In general, these methods can be classified into three broad categories: (1) subchannel analysis; (2) porous medium formulation; and, (3) benchmark rod-bundle thermal-hydraulic analysis.

A. Subchannel Analysis

The subchannel method is the most widely used in rod-bundle thermal-hydraulic analysis to date. Historically, and as originally intended, subchannel analysis has been used primarily for design calculations; it explicitly assumes that one of the velocity components (axial velocity in z-direction) is dominant, compared to components in the other directions (crossflows in x and y directions). Thus, it is advantageous from both physical and computational points of view to treat axial and transverse momentum equations separately so that some simplifications can be applied to the transverse momentum equations.

Until recently, the subchannel method also has been employed in reactor safety analysis; e.g., to resolve flow-blockage problems in a fuel assembly. In this case, the usual assumptions for small cross-flows in transverse directions are no longer valid, and numerical solution techniques for the initial value problem cannot be applied. A typical subchannel arrangement of a 19-pin rod bundle, control volume for axial momentum equation and control volumes for axial and transverse momentum equations are shown in Figs. 1(a), 1(b), and 1(c) respectively. The transverse momentum equations used in the THI3D [1], COBRA-IIIC [2], SABRE-1 [3] codes are listed in Table I.

1. Basic Limitations

(1) The fine structure of both velocity and temperature within a subchannel is ignored (lumped parameter approach).

(2) The transverse momentum equations cannot be treated with the same rigor as the axial momentum equation because of the nonorthogonal char-

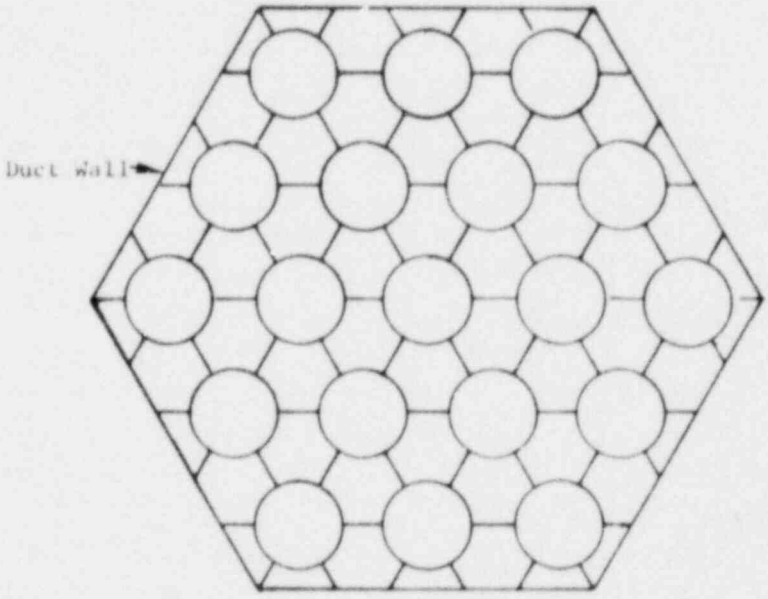

a. Typical Subchannel Arrangement

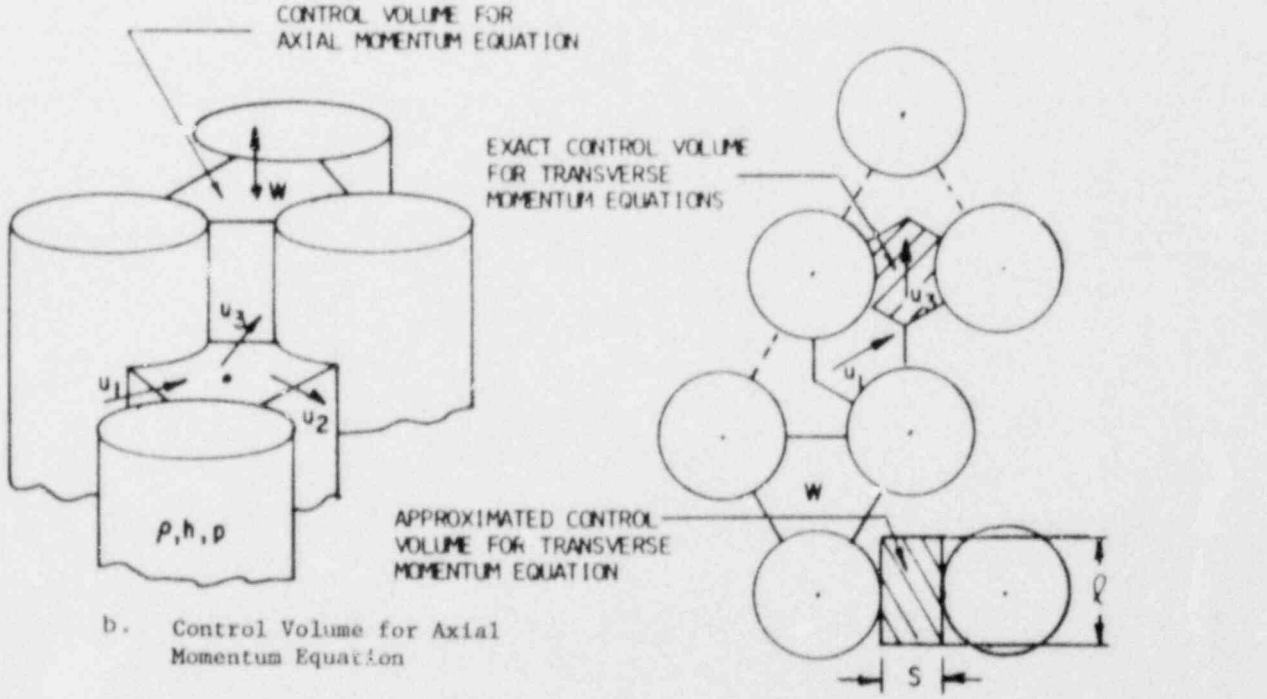

b. Control Volume for Axial Momentum Equation

c. Control Volumes for Axial and Transverse Momentum Equations

Fig. 1. Subchannel Arrangement and Control Volumes for Axial and Transverse Momentum Equations

TABLE I. COMPARISON OF TRANSVERSE MOMENTUM EQUATIONS USED IN VARIOUS COMPUTER PROGRAMS

THI3D

$$0 = - \frac{\partial w^{*} m_{ij}}{\partial z} + \frac{\partial u_i m_{ij}}{\partial x_i} - S \frac{\partial P}{\partial x_i} + F_{ij}$$

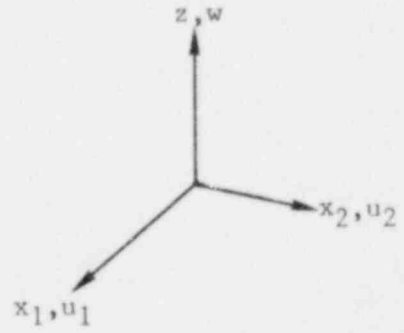

COBRA-IIIC**

$$\frac{\partial m_{ij}}{\partial t} = - \frac{\partial w^{*} m_{ij}}{\partial z} + \frac{S}{\ell} (P_i - P_j) - F_{ij}$$

SABRE-1***

$$0 = - \frac{\partial \rho u_i w}{\partial z} - \lambda \frac{\partial \rho u_i^2}{\partial x_i} - \frac{\partial P}{\partial x_i} + \mu \frac{\partial^2 u_i}{\partial z^2} + R_i$$

COMMIX-1

$$\gamma_V \frac{\partial \rho u_i}{\partial t} = - \frac{\partial \gamma_z \rho u_i w}{\partial z} - \frac{\partial \gamma_j \rho u_i u_j}{\partial x_j} - \gamma_V \frac{\partial P}{\partial x_i} + \frac{\partial}{\partial z} \gamma_z \mu \frac{\partial u_i}{\partial z} + \frac{\partial}{\partial x_j} \gamma_j \mu \frac{\partial u_i}{\partial x_j} + R_i$$

① ② ③ ④ ⑤ ⑥ ⑦

Computer Program	1	2	3	4	5	6	7
COMMIX-1	yes	yes	yes	yes	yes	yes	yes
THI3D-1	no	yes	yes	yes	no	no	yes
COBRA-IIIC	yes	yes	no	yes	no	no	yes
SABRE-1	no	yes	yes	yes	yes	no	yes

Note:

F_{ij} = force per unit area

λ = geometrical factor to account for the difference between the exact control volume and the approximated control volume for the transverse momentum equation [see Fig. 1(c)].

** COBRA-IV neglects the cross product of transverse velocity components and fluid to fluid shear forces.

*** The latest version of the SABRE code has transient capability.

acteristics of subchannel arrangement. Specifically, the finite-difference representation of the second derivatives cannot be rigorously evaluated.

(3) To facilitate calculations, approximations are necessary for simplifying the geometric configuration of the control volume used in the transverse momentum equation and interfacing the required information at various locations between control volumes for the axial and transverse momentum equations.

2. Mathematical Model

The following governing equations, boundary conditions, and solution technique are reproduced from Ref. 1; extension to transient formulations is straightforward.

a. Conservation of Mass

$$\frac{\partial m_{z,i}}{\partial z} = - \sum_{j=1}^{N} m_{ij}, \tag{1}$$

where

$m_z = \rho w A_z$ = axial flow rate,

ρ = coolant density,

w = axial velocity,

A_z = axial flow area,

$m_{ij} = \rho u_{ij} A_{ij}/\Delta z$ = diversion crossflow rate per unit height between subchannels i and j (wire-wrap sweeping crossflow can be included),

u_{ij} = transverse velocity in x_j direction,

A_{ij} = crossflow area between subchannel i and j,

Δz = axial increment,

and

N = number of neighboring subchannels.

b. Conservation of Momentum

As mentioned before, the momentum equation is subdivided into the axial momentum equation and the transverse momentum equations so that the latter can be treated with simplified assumptions:

b.1 Axial Momentum

$$\frac{\partial P_i A_{z,i}}{\partial z} = \sum_{j=1}^{N} \left[m_{ij} w^* + (m_{ij} + m'_{ij})(w_i - w_j) \right] - \left[\rho_i g + \left(\frac{m_{z,i}}{A_{z,i}} \right)^2 \left(\frac{f}{2D\rho_i} + \frac{k}{2\rho_i \Delta z} + \frac{A_{z,i}}{\bar{A}_{z,i}} \frac{\partial}{\partial z} \frac{1}{\rho_i} - \frac{1}{\rho_i \bar{A}_{z,i}} \frac{\partial A_{z,i}}{\partial z} \bar{A}_{z,i} \right) \right] , \qquad (2)$$

where

g = gravitational constant,

f = friction factor,

k = form loss coefficient,

D = equivalent hydraulic diameter,

P = pressure,

m'_{ij} = turbulent crossflows between subchannels i and j per unit height, including natural turbulence and turbulence promoted by the presence of wire wrap,

$$\bar{A}_z = \int_0^{\Delta z} A_z(z)dz/\Delta a \ ,$$

$$w^* = \frac{w_i + w_j}{2} \ ,$$

and the asterisk denotes the quantity associated with the donor subchannel.

b.2 Transverse Momentum

If the interactions between the transverse momentum in the direction under consideration and the other transverse direction (or directions) are neglected,* the transverse momentum equation may be written as

$$\frac{\partial m_{ij} w_i}{\partial z} + \frac{\partial m_{ij} u_i}{\partial x_j} = \left(- \frac{\partial P}{\partial x_j} + \frac{F_{x_j}}{V} \right) S_j, \quad j = 1, 2, \ldots, N, \qquad (3)$$

where

---

* An attempt to include both the transverse momentum flux gradients and their interactions in principal directions has been formulated and presented in THI3D-1[1].

x_j = transverse direction along the centroids of subchannels i and j,

V = elementary volume,

and

S_j = crossflow width between subchannels i and j.

The general surface force term F_{x_j} may be approximated by

$$F_{x_j} = - \frac{\tilde{k} |m_{ij}| m_{ij}}{2\rho_i S^2_j \Delta x_j} V \quad ,$$

where

$\tilde{k}$ = crossflow resistance,

and

Δx_j = centroid distance between subchannels i and j in the x_j direction.

c. Conservation of Energy

$$\frac{\partial h_i}{\partial z} = \frac{1}{m_{z,i}} \sum_{j=1}^{N} \left[\frac{S_j}{\Delta x_j} \kappa (T_j - T_i) + \delta (m_{ij} + c'_{ij} - c'_{ij})(h_i - h_j) \right]$$

$$+ \left(q'''_i - \frac{\delta_l q'_{d,i}}{A_{d,i}} \right) \frac{\bar{A}_{z,i}}{m_{z,i}} \quad , \qquad (4)$$

where

h = coolant enthalpy,

T = coolant temperature,

κ = thermal conductivity of coolant,

c'_{ij} = turbulent-exchange coefficient per unit height,

q''' = heat generation per unit volume per unit time,

q'_d = heat loss per unit height per unit time through the duct wall,

A_d = heat-transfer area through the duct wall,

δ = 0 for crossflows leaving channel i to j,

= 1 for crossflows entering channel i from j,

and

δ_l = 0 for channels located away from the duct wall,

= 1 for channels located next to the duct wall.

Both m'_{ij} and c'_{ij} can be combined into a single turbulent exchange coefficient (i.e., $am_{ij} = m_{ij} - c_{ij}$, where a is a constant), since m'_{ij} and c'_{ij} cannot be distinguished through experimental measurements.

d. Boundary Conditions

The pressure drop boundary condition is used. Inlet pressure, coolant densities, and temperatures (or enthalpies) of all subchannels are assumed to be known. Inlet pressures can be specified as either uniform or nonuniform for all subchannels, but outlet pressures must be uniform. To satisfy the uniform outlet pressures, inlet velocities of all subchannels must be adjusted, using the following iterative solution technique.

3. Solution Technique

Coolant parameters are calculated simultaneously for all subchannels, by starting at the bottom of the core and moving upward, stepwise. Coolant enthalpies (temperatures), pressures, densities at the inlet, and heat-flux distributions in all subchannels are known. Inlet velocities are first assumed to be known, and then solved iteratively. Crossflows are computed based on coolant properties at the bottom of the step length. Knowing the crossflows within the step and the heat addition into the step, the change in coolant enthalpy (temperatures), pressure, density, and velocity can be determined successively for each step length. To account for the effect of local pressure drop on coolant properties, an iteration within each step length must be performed. Thus, a consistent set of local thermodynamic properties of the coolant can be maintained.

The resulting enthalpy, pressure, density, and velocity at the top of the step length are used as input to the next step length. This procedure is continued until the top of the core is reached. Accordingly, the pressure at the top of the core may be expressed as a function of inlet pressures, densities, and velocities of all subchannels:

$$P_j^o = P_j^o\left(w_1^i, w_2^i, \ldots, w_M^i; \rho_1^i, \rho_2^i, \ldots, \rho_M^i; P_1^i, P_2^i, \ldots, P_M^i\right)$$

$$j = 1, 2, \ldots, M, \qquad (5)$$

where superscripts i and o correspond to inlet and outlet values; P, w, and ρ are pressure, axial coolant velocity, and density, respectively; and M is the number of subchannels under consideration.

The total derivative of Eq. (5) can be written

$$dP_j^o = \sum_{k=1}^{M} \left(\frac{\partial P_j^o}{\partial w_k^i} dw_k^i + \frac{\partial P_j^o}{\partial \rho_k^i} d\rho_k^i + \frac{\partial P_j^o}{\partial P_k^i} dP_k^i \right). \tag{6}$$

For practical purposes in reactor design, both the inlet pressure and the coolant-density distribution are assumed to be known. A set of inlet velocities must be determined to satisfy the uniform pressure at the exit of all subchannels. Basic equations for conservation of mass, energy, and momentum are used to compute the outlet pressure distribution for a given set of inlet coolant velocity conditions. Interaction between subchannels is taken into account by allowing for crossflow through adjacent subchannels. The amount of crossflow is expressed as a function of pressure, and temperature or enthalpy gradient of the adjacent subchannels at the same elevation. Equation (6) can now be expressed in the matrix form

$$[dP^o] = [B][dw^i], \tag{7}$$

where

$[dP^o]$ = column matrix with elements dP_j^o,

$[B]$ = M x M Jacobian matrix with elements $\partial P_j^o / \partial w_k^i$,

and

$[dw^i]$ = column matrix with elements dw_k^i .

If $[B]$ is a nonsingular matrix, Eq. (7) can be written

$$[\Delta w^i] = [B]^{-1}[\Delta P^o].$$

Equation (7) couples with the following boundary conditions:

At the top of the core:

P_j^o = constant, j = 1, 2, ..., M.

At the bottom of the core:

(1) P_j^i = constant, or a known distribution, j = 1, 2, ..., M,

(2) T_j^i = inlet tempeature or h_j^i (inlet enthalpy) are known at j = 1, 2, ..., M,

and

(3) $$\sum_{j=1}^{N} \rho_j^i A_{z,j}^i w_j^i = \text{constant},$$

where $A_{z,j}$ is the axial coolant flow area of subchannel j.

Boundary condition (3) can be considered a constraint of Eq. (8), which can be written:

$$[\Delta w^i] = [B]^{-1}[\Delta P^o] + \lambda\,[B]^{-1}[I], \tag{9}$$

where $[I]$ is a unit column matrix, and λ is a scalar or Lagrangian multiplier to be determined.

Multiplying Eq. (9) by $[A]$ and $[\rho]$ gives

$$\lambda = -\frac{[A][\rho][B]^{-1}[\Delta P^o]}{[A][\rho][B]^{-1}[I]}\quad , \tag{10}$$

where $[A]$ is a row matrix of the axial coolant flow area at the inlet, $[\rho]$ is a square diagonal matrix of the coolant density at the inlet, and $[A][\rho][\Delta w^i] = 0$.

In practice, the inlet velocity of the first subchannel is changed by a preassigned small magnitude, and resulting changes in outlet pressure $[\Delta P^o]$ for all subchannels are then determined. Elements of the first column of the Jacobian matrix $[B]$ are determined from this calculation. The original velocity distribution is restored, and the procedure is repeated for each subchannel. The inverse of matrix $[B]$ is then determiined, and λ is calculated using Eq. (10). Knowing λ, $[\Delta w^i]$ in Eq. (9) is then determined. The new inlet velocity distribution can now be obtained from

$$[w^i_{NEW}] = [w^i] + [\Delta w^i]\quad , \tag{11}$$

where $[w^i_{NEW}]$ and $[w^i]$ are column matrices of the new and original inlet axial velocities, respectively.

A simplified computational logic diagram of subchannel analysis is presented in Fig. 2.

B. Porous Medium Formulation

A set of quasi-continuum governing equations for conservation of mass, momentum and energy for a finite control volume is derived from both integral and differential approach. The derivation of both the integral and differential aproach can be found in ref. 4. The system consists of a single-phase fluid with discrete stationary solid structures. Volume porosity, surface permeabilities, distributed resistance and distributed heat source (or sink) are systematically included in the derivation.

The concept of volume-porosity and distributed-resistance and heat-source arises naturally in the local volume averaging process [5,6]. The size of control volume used in the local volume average must be small, compared to the large-scale phenomena of interest. Distributed resistance alone is normally used to characterize anisotropy of a porous medium. However, when local flow area (or path) changes abruptly, and high resolution of local temperature and velocity distribution is needed, additional delineation of the anisotropic characteristics of the medium is necessary. Thus, a new approach with volume porosity, surface permeability, and distributed resistance and heat source is

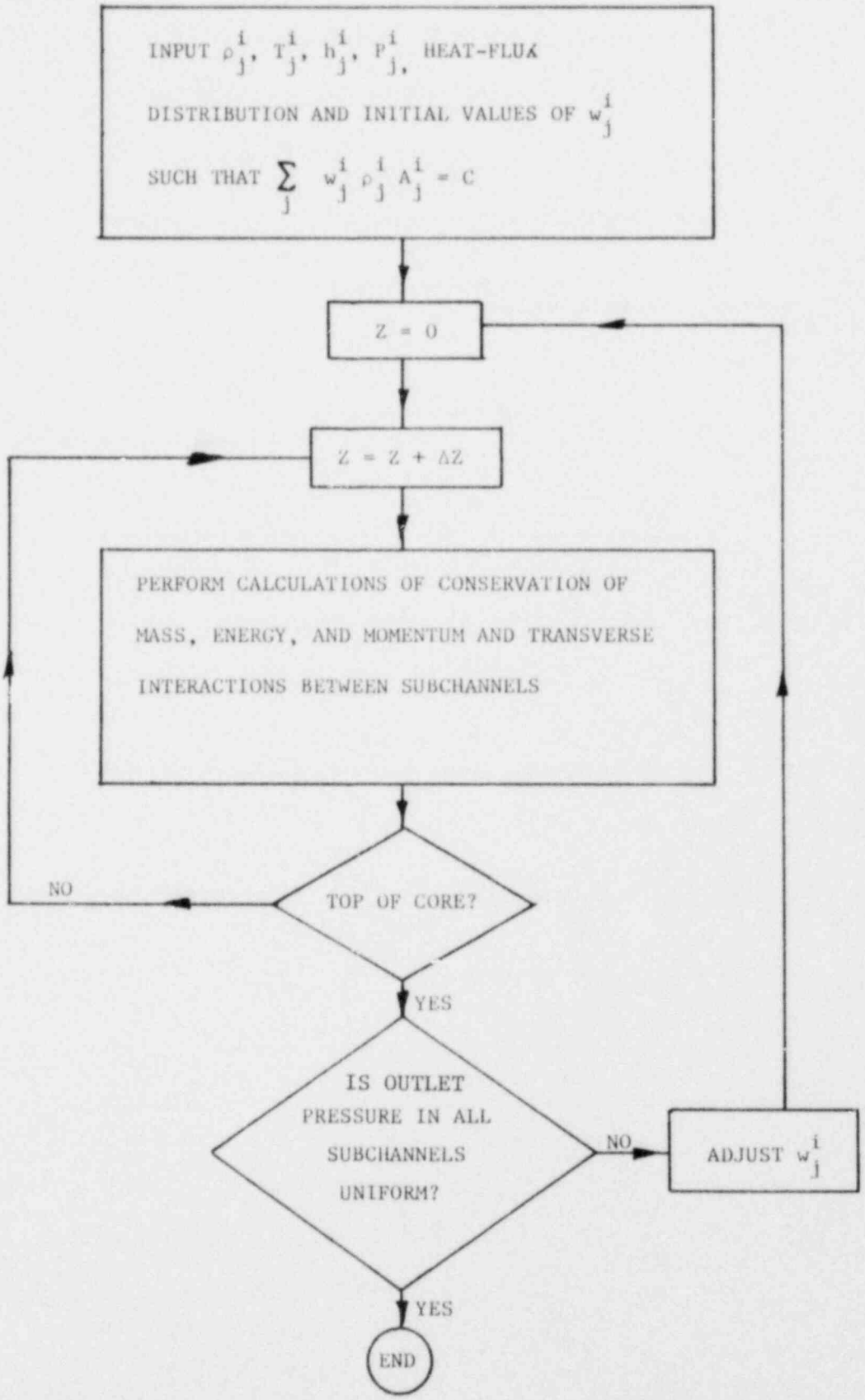

Fig. 2. Simplified Computational Logic Diagram of Subchannel Analysi

developed. The concept of surface permeability is new in porous medium formulation [4,7], and it greatly facilitates the modeling of anisotropic effect of a medium. Now, the anisotropic characteristics of rod bundles can be modelled by using appropriate local surface permeability and distributed resistance. It is important to note that the concept of surface permeability, when properly applied, will reduce the inaccuracy in the calculated volume averaged velocity and temperature due to replacing the discrete fluid resistance and heat source (or sink) of the physical system by an idealized distributed system. The surface permeability is usually known, while the distributed resistance is, in general, not well defined. This is particularly true for the analysis of reactor components where geometrically complicated structures are often encountered.

Recently, the COMMIX-1 code[7], which employs the porous medium approach with volume porosity, surface permeability, distributed resistance and distributed heat source was developed. The typical mesh structure for a rod-bundle used in the COMMIX-1 code is shown in Fig. 3. The transverse momentum equations used in the COMMIX-1 code are presented in Table I along with those of the other codes for comparison.

1. Basic Limitations

The unique advantages of the volume-porosity, surface-permeability, and distributed resistance and distributed heat source approach presented in this section are the use of orthogonal coordinates and geometrically similar control volumes. Thus, limitations (2) and (3) employed in the subchannel analysis are eliminated; however, limitation (1) is still retained. It is to be noted that just as the friction factor must be calibrated in subchannel analysis, so must the distributed resistance be calibrated with experimental data in the porous medium formulation.

2. Derivation of Quasi-Continuum Governing Equations

In a recent publication [4], a set of quasi-continuum equations was presented for the conservation of mass, momentum and energy for a system consisting of a single-phase fluid and dispersed, stationary solid structures. The results were derived from a local integral formulation. In this investigation, the macroscopic transport equations are obtained by averaging the microscopic transport equations over a local volume and use is made of the averaging theorems developed almost simultaneously by Slattery [5,8,9] and by Whitaker [10,11]. The concept of volume porosity, surface permeability, distributed resistance and distributed heat source arises naturally.

Consideration is hereby given to a region consisting of a single-phase fluid with stationary structures. Heat may be generated or absorbed by the structures. For an arbitrary point in the region, we associate a closed surface A whose Volume is V. A portion of V that contains the fluid is V_f and the total fluid-solid interface is A_{fs}. A portion of A through which the fluid may flow is A_e. A schematic of the system just described is illustrated in Fig. 3.

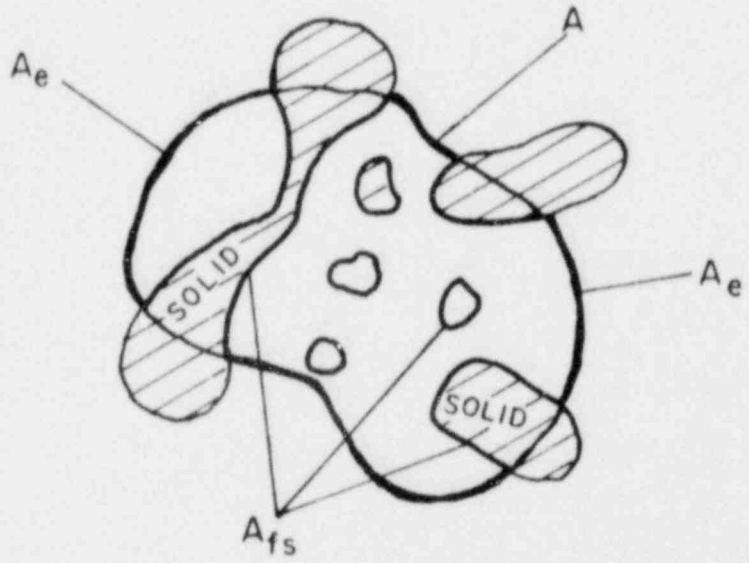

Fig. 3. Local Volume Average of Physical System

a. Local Volume Average, Intrinsic Average and Area Average

Let ψ be any intensive property associated with the fluid. It may be a scalar, vector or second-order tensor. The local volume average of ψ is defined by:

$$^{3}\langle\psi\rangle \triangleq \frac{1}{V}\int_{V} I(\vec{p})\,\psi dV \quad . \tag{12}^{*}$$

where $\vec{p}$ is the position vector and the indicator function, $I(\vec{p})$ is defined by:

$$I(\vec{p}) = \begin{array}{l} 1, \text{ if the end point of p is in fluid} \\ 0, \text{ if the end point of p is in solid} \end{array} \tag{13}$$

An equivalent form of Eq. (12) is

$$^{3}\langle\psi\rangle = \frac{1}{V}\int_{V_f} \psi dV \quad . \tag{12a}$$

The intrinsic local volume average of ψ is

$$^{3i}\langle\psi\rangle \triangleq \frac{1}{V_f}\int_{V_f} \psi dV \quad . \tag{14}^{**}$$

Likewise, the local area average of ψ is

$$^{2}\langle\psi\rangle \triangleq \frac{1}{A}\int_{A} I(\vec{\rho})\,\psi dA = \frac{1}{A}\int_{A_f} \psi dA \quad , \tag{15}$$

where A_f denotes the portion of A that is occupied by the fluid. The associated intrinsic area average is

$$^{2i}\langle\psi\rangle \triangleq \frac{1}{A_f}\int_{A_f} \psi dA \quad . \tag{16}$$

It is important to note that in Eq. (15) the area A under consideration may not be the total enclosing surface. (If A is the enclosing surface in its entirety, then A_f in Eqs. (15) and (16) should be replaced by A_e; see Fig. 3). In fact, one often concerns with a designated portion of it. For instance, in Cartesian coordinate system, the averaging volume may be selected to be a parallelepiped $\Delta x\Delta y\Delta z$. The average mass flux through the surface ΔA_x

---

* The superscript ^{3} designates that the average is associated with volume. We shall use superscripts ^{2} and ^{1} for area and line (segment) averages.

** The superscript i denotes intrinsic average.

(area $\Delta y \Delta z$) whose normal points in the direction of positive x-axis is

$$2(x)_{\langle \rho u \rangle} = \frac{1}{\Delta A_x} \int_{\Delta A_x} I(\vec{p}) \rho u dA \quad ,$$

$$= \frac{1}{\Delta A_{x,f}} \int_{\Delta A_{x,f}} \rho u dA \quad , \tag{15a}$$

where $\Delta A_{x,f}$ denotes the fluid portion of ΔA_x. The corresponding intrinsic average is

$$2i(x)_{\langle \rho u \rangle} = \frac{1}{\Delta A_{x,f}} \int_{\Delta A_{x,f}} \rho u dA \quad . \tag{16a}$$

b. Volume Porosity and Surface Permeability

The rates of fluid volume V_f to the total volume V is defined to be the volume porosity, γ_v. Thus,

$$\gamma_v \triangleq \frac{V_f}{V} \quad . \tag{17}$$

Since $V_f = \int_V I(\vec{p}) dV$, γ_v can also be written as

$$\gamma_v = \frac{1}{V} \int_V I(\vec{p}) dV \quad . \tag{17a}$$

Furthermore,

$$^3\langle \psi \rangle = \gamma_v \, ^{3i}\langle \psi \rangle \quad . \tag{18}$$

Analogously, we define the surface permeability γ_A associated with <u>any</u> surface (not necessarily closed) as,

$$\gamma_A \triangleq \frac{A_f}{A} = \frac{1}{A} \int_A I(\vec{p}) dA \quad , \tag{19}$$

where A_f is the portion of A that is occupied by the fluid. Consider, for example, the surface ΔA_x described in Section a. The surface permeability is

$$\gamma_{A_x} \triangleq \frac{\Delta A_{x,f}}{\Delta A_x} = \frac{1}{\Delta A_x} \int_{\Delta A_x} I(\vec{p}) dA \quad . \tag{20}$$

Clearly,

$$^2\langle \psi \rangle = \gamma_A \, ^{2i}\langle \psi \rangle \quad . \tag{21}$$

c. Local Volume-Averaged Transport Equations

c.1 Equation of Mass Conservation

The differential equation governing mass conservation for the fluid is

$$\frac{\partial \rho}{\partial t} + \nabla \cdot \rho \vec{v} = 0 \quad , \tag{22}$$

where ρ = fluid density,

t = time,

and

$\vec{v}$ = fluid velocity vector.

Taking the volume average of Eq. (22) as defined by Eqs. (12) or (12a) yields

$$^3\left\langle \frac{\partial \rho}{\partial t} \right\rangle + {}^3\langle \nabla \cdot \rho \vec{v} \rangle = 0 \quad . \tag{23}$$

Application of the general transport theorem [13] to the first term in Eq. (23) yields

$$^3\left\langle \frac{\partial \rho}{\partial t} \right\rangle = \frac{\partial {}^3\langle \rho \rangle}{\partial t} - \frac{1}{V} \int_{A_{fs}} \rho \vec{v}_{fs} \cdot \hat{n} dA \quad , \tag{24}$$*

where $\vec{v}_{fs}$ is the velocity of A_{fs}, and $\hat{n}$ is the unit outdrawn normal vector on A_{fs} and away from the fluid. For the case under study, $\vec{v}_{fs} = 0$ since the solids are fixed. It is interesting to note that the integral in Eq. (24) may vanish even if $\vec{v}_{fs} \neq 0$ everywhere on A_{fs}. This would occur if the solids that are completely inside A are nondeformable in motion relative to the fluid, since for any interior solid of surface ΔA_{fs}, $\int_{\Delta A_{fs}} \rho \vec{v}_{fs} \cdot \hat{n} dA = 0$ if the variation of fluid density over ΔA_{fs} is negligible.

In either case,

$$^3\left\langle \frac{\partial \rho}{\partial t} \right\rangle = \frac{\partial {}^3\langle \rho \rangle}{\partial t} = \gamma_v \frac{\partial {}^{3i}\langle \rho \rangle}{\partial t} \quad . \tag{24a}$$

Applying the theorem of local volume averaging to a divergence due to Slattery [5,8] and Whitaker [11,14] gives

---

* In general, the velocity of the fluid-solid interface $\vec{v}_{fs}$ may not be identical to the fluid velocity v at the interface. This would occur when mass transfer takes place.

$$^{3}\langle \nabla \cdot \rho\vec{v} \rangle = \nabla \cdot {}^{3}\langle \rho\vec{v} \rangle + \frac{1}{V} \int_{A_{fs}} \rho\vec{v} \cdot \hat{n} dA \quad . \tag{25}$$

Again, the second term on the right hand side of Eq. (25) vanishes because, for the problem under consideration, $\vec{v} = 0$ everywhere on A_{fs}. Consequently,

$$^{3}\langle \nabla \cdot \rho\vec{v} \rangle = \nabla \cdot {}^{3}\langle \rho\vec{v} \rangle = \frac{1}{V} \nabla \cdot \int_{V_f} \rho\vec{v} dV \quad .$$

Since, as has been shown, by Slattery [5], for any quantity B which may be a scalar, vector, or tensor,

$$\nabla \int_{V_f} B dV = \int_{A_e} \hat{B} n dA \quad , \tag{26}$$

it follows then

$$^{3}\langle \nabla \cdot \rho\vec{v} \rangle = \frac{1}{V} \int_{A_e} \rho\vec{v} \cdot \hat{n} dA \quad . \tag{27}$$

Substituting Eqs. (24a) and (27) into Eq. (23) yields,

$$\boxed{\gamma_v \frac{\partial {}^{3}i\langle \rho \rangle}{\partial t} + \frac{1}{V} \int_{A_e} \rho\vec{v} \cdot \hat{n} dA = 0} \quad , \tag{28}$$

which is the required volume averaged mass conservation equation. The need of introducing the concept of surface permeability is suggested by the second term of Eq. (28) and others in the momentum and energy equations.

c.2 Linear Momentum Equation

We begin with the dynamic equation of fluid motion;

$$\frac{\partial(\rho\vec{v})}{\partial t} + \nabla \cdot (\rho\vec{v}\vec{v}) = \rho\vec{g} - \nabla p + \nabla \cdot \bar{\bar{\tau}} \quad , \tag{29}$$

where $\vec{g}$ = body force per unit fluid mass; in the gravitational field, it is simply the gravitational acceleration vector,

p = static pressure,

and

$\bar{\bar{\tau}}$ = stress tensor.

Performing the local volume averaging of Eq. (29) gives

$$^{3}\left\langle \frac{\partial(\rho\vec{v})}{\partial t} \right\rangle + {}^{3}\langle \nabla \cdot (\rho\vec{v}\vec{v}) \rangle = {}^{3}\langle \rho \rangle \vec{g} - {}^{3}\langle \nabla p \rangle + {}^{3}\langle \nabla \cdot \bar{\bar{\tau}} \rangle \quad , \tag{30}$$

with the aid of the general transport theorem, the theorem of volume averaging, Eq. (26) and recognizing that $\vec{v}_{fs}$ and $\vec{v}$ vanish on A_{fs}, Eq. (30) can be rewritten

$$\gamma_v \frac{\partial}{\partial t} {}^{3i}\langle\rho\vec{v}\rangle + \frac{1}{V}\int_{A_e} \rho\vec{v}\,(\vec{v}\cdot\hat{n})\,dA = \gamma_v\,{}^{3i}\langle\rho\rangle\vec{g} + \frac{1}{V}\int_{A_e}\left(-p\hat{n} + \bar{\bar{\tau}}\cdot\hat{n}\right)dA - \gamma_v\,{}^{3i}\langle\vec{R}\rangle \quad , \tag{31}$$

in which $\vec{R}$ is the resistance force exerted on the fluid by the dispersed solid per unit volume of the fluid. In writing Eq. (31), use has been made of the following relationship

$$\int_{A_{fs}}\left(-p\hat{n} + \bar{\bar{\tau}}\cdot\hat{n}\right)dA = -\int_{V_f}\vec{R}\,dV \quad , \tag{32}$$

which may be regarded as the defining equation for $\vec{R}$. The negative sign is introduced to convey the notion that such force retards the motion. Equation (31) is the volume averaged linear momentum equation for the system under consideration.

The surface permeability concept is introduced in the second term of the right hand side (RHS), and the second term of the left hand side (LHS) of Eq. (31).

c.3 Equations of Energy Conservation

c.3.1 Energy Equation in Terms of Internal Energy

The differential transport equation for internal energy is

$$\frac{\partial(\rho e)}{\partial t} + \nabla\cdot(\rho e\vec{v}) = -p\nabla\cdot\vec{v} - \nabla\cdot\vec{q} + \dot{Q} + \Phi \quad , \tag{33}$$

where e = internal energy per unit fluid mass,

$\vec{q}$ = heat flux vector,

$\dot{Q}$ = rate of internal heat generation per unit fluid volume due to extraneous heat source,

and

Φ = dissipation rate of mechanical energy into heat.

The local volume average of Eq. (33) is

$${}^{3}\left\langle\frac{\partial(\rho e)}{\partial t}\right\rangle + {}^{3}\langle\nabla\cdot(\rho e\vec{v})\rangle = -{}^{3}\langle p\nabla\cdot\vec{v}\rangle - {}^{3}\langle\nabla\cdot\vec{q}\rangle + {}^{3}\langle\dot{Q}\rangle + {}^{3}\langle\Phi\rangle \quad . \tag{34}$$

Again, with the aid of the general transport theorem, the theorem of volume averaging, etc., we obtain the local volume averaged internal energy equation:

$$\gamma_v \frac{\partial}{\partial t} {}^{3i}\langle \rho e \rangle + \frac{1}{V} \int_{A_e} \rho e \vec{v} \cdot \hat{n} dA = - \gamma_v {}^{3i}\langle p \nabla \cdot \vec{v} \rangle + \frac{1}{V} \int_{A_e} \kappa \cdot \hat{n} \cdot \nabla T dA + \gamma_v \left({}^{3i}\langle \dot{Q}_{rb} \rangle + {}^{3i}\langle \dot{Q} \rangle + {}^{3i}\langle \Phi \rangle \right) \quad (35)$$

in which the heat flux vector $\vec{q}$ is taken to be $- \kappa \nabla T$, κ being the fluid conductivity. $\dot{Q}_{rb}$ denotes the rate of heat liberation from the dispersed solids per unit volume of the fluid. Thus

$$\int_{V_f} \dot{Q}_{rb} dV = - \int_{A_{sf}} \vec{q} \cdot \hat{n} dA \quad . \quad (36)$$

c.3.2 Energy Equation in Terms of Enthalpy

The differential equation for the transport of static enthalpy $h \left(= e + \frac{p}{\rho} \right)$ is

$$\frac{\partial (\rho h)}{\partial t} + \nabla \cdot (\rho h \vec{v}) = \frac{dp}{dt} - \nabla \cdot \vec{q} + \dot{Q} + \Phi \quad , \quad (37)$$

and the volume averaged enthalpy equation is

$$\gamma_v \frac{\partial}{\partial t} {}^{3i}\langle \rho h \rangle + \frac{1}{V} \int_{A_e} \rho h \vec{v} \cdot \hat{n} dA = \gamma_v {}^{3i}\left\langle \frac{dp}{dt} \right\rangle + \frac{1}{V} \int_{A_e} \kappa n \cdot \nabla T dA + \gamma_v \left({}^{3i}\langle \dot{Q}_{rb} \rangle + {}^{3i}\langle \dot{Q} \rangle + {}^{3i}\langle \Phi \rangle \right) . \quad (38)$$

Since,

$$\frac{dp}{dt} = \frac{\partial p}{\partial t} + \nabla \cdot (p \vec{v}) - p \nabla \cdot \vec{v} \quad ,$$

$${}^{3i}\left\langle \frac{dp}{dt} \right\rangle = \frac{\partial {}^{3i}\langle p \rangle}{\partial t} + \nabla \cdot {}^{3i}\langle p \vec{v} \rangle - {}^{3i}\langle p \nabla \cdot \vec{v} \rangle \quad .$$

Again, the surface permeability appears in the second term of RHS and the second term of LHS of Eq. (38).

3. Initial and Boundary Conditions

Initial conditions are obtained either by specifying the fluid velocity, temperature and pressure distribution throughout the interior points of

the space under consideration, or by continuing a previous computer run via a restart capability. Once the fluid temperature and pressure are specified, as in the former case, the corresponding density and enthalpy are calculated from equations of state. Boundary conditions are specified with appropriate temperature, velocity, and heat flux distributions at all external boundaries.

4. Numerical Technique

The quasi-continuum governing equations, Eqs. (28), (31), and (38) are finite differenced in a staggered mesh system[12]. The pressure (P), temperature (T), enthalpy (h), density (ρ), and volume porosity (γ_V) are defined at cell centers. The velocity $\vec{v}$ and surface permeability (γ_x, γ_y, and γ_z in x, y, and z directions, respectively) are defined at the center of each cell surface. The finite difference equations are solved by using ICE (Implicit Continuous-fluid Eulerian) procedure with rebalance. The rebalance technique has been developed by us and is an integral mass balance of a local region related to the local pressure correction. A simplified computational logic diagram of COMMIX-1 is shown in Fig. 4. Some pertinent numerical results obtained from the COMMIX-1 code are presented in the paper by Domanus, Shah, and Sha in a special issue on Liquid Metal Fast Breeder Reactor (LMFBR) Single-Phase Rod-Bundle Thermal-Hydraulics of Nuclear Engineering and Design [15], which will be published soon.

5. Unique Features

The COMMIX-1 computer program has three unique features: one is that the model is capable of treating both continuum (e.g., reactor plenum, piping mixing) and quasi-continuum (e.g., rod bundle or fuel assembly) systems by introducing porous medium formulation with volume porosity and surface permeability, as well as distributed resistance and heat source. This capability represents the most cost-effective way of handling two classes of problems by a single computer program. Second is the concept of surface permeability which is new in porous medium formulation, and it greatly facilitates accounting for the anisotropic effects in a medium. Third, it can properly model the diffusion term in momentum equations which is lacking in the present subchannel analysis. The other is the inclusion of the local mass residue effect [5] in the energy and momentum equations and the development of rebalance technique in the solution procedure. As a result of this inclusion, both the convergence rate and accuracy are greatly improved.

C. Benchmark Rod-Bundle Thermal-Hydraulic Analysis

The fine structure of both velocity and temperature within a subchannel or a computational cell is ignored in the subchannel analysis and the porous medium approach. However, this fine structure can be accounted for through the specification of rods as internal boundary conditions. Recently, BODYFIT-1, a three-dimensional, transient, single-phase component computer program[16,17,18], has been developed. It utilizes boundary-fitted coordinates to transform a complicated rod-bundle geometry into a rectangular coordinate mesh system as shown in Fig. 5. Note that all the governing equations are transformed accordingly into new variables (transformed space) before being approximated by finite difference equations which are solved in the usual manner [7].

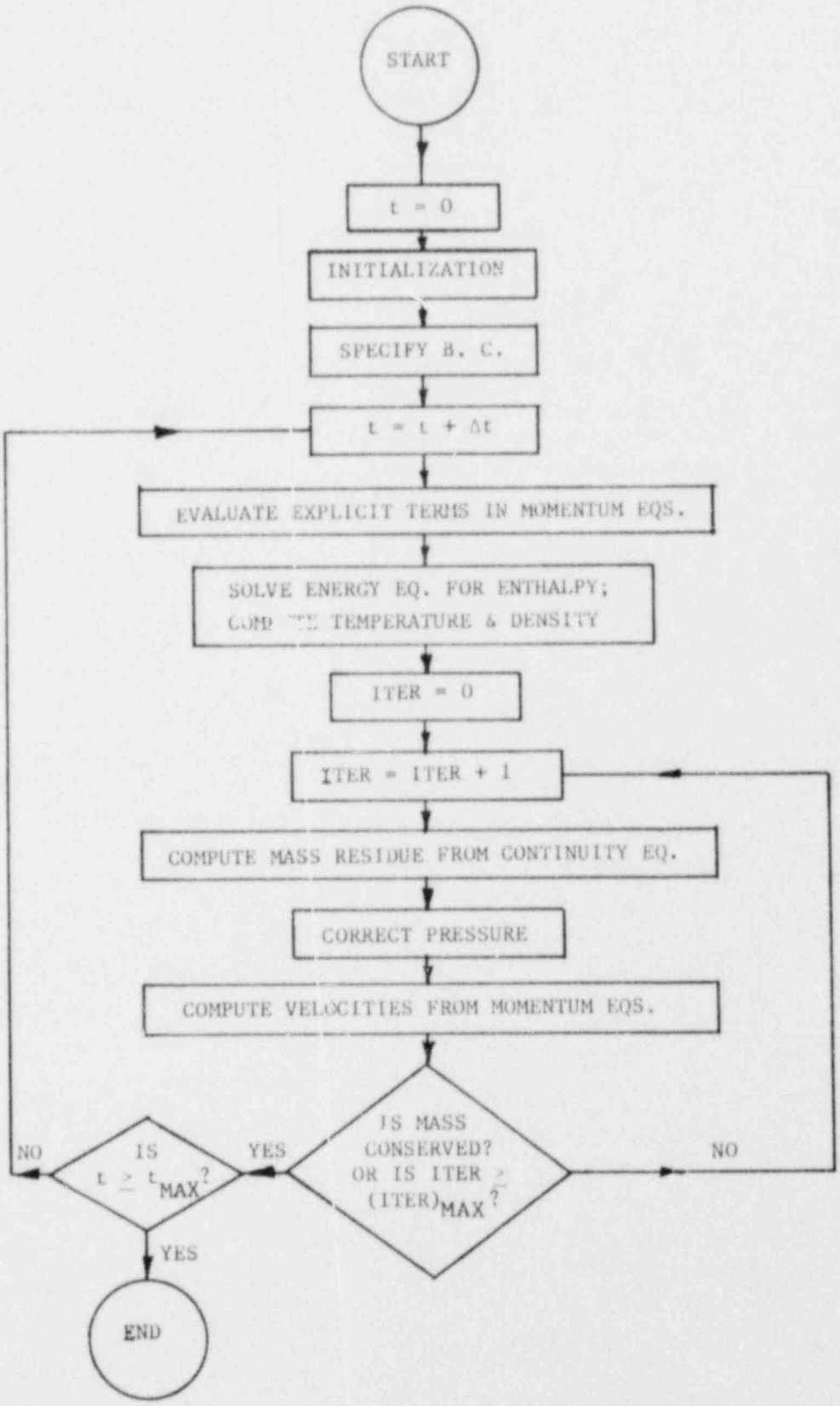

Fig. 4. Simplified Computational Logic Diagram of COMMIX-1

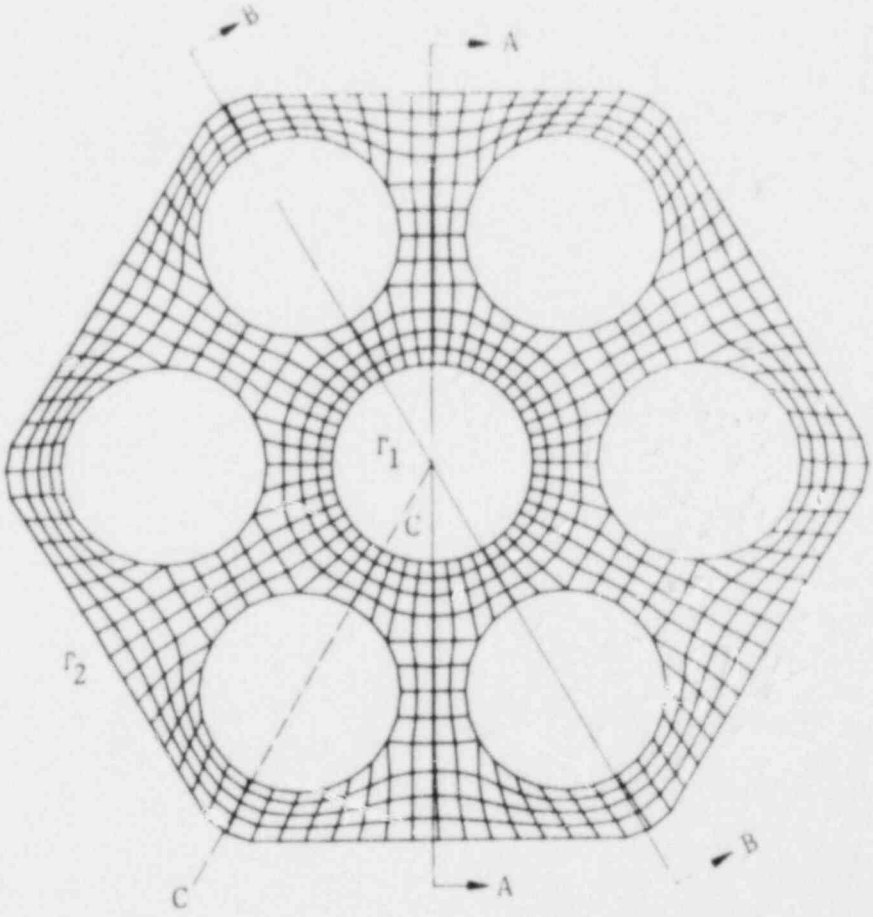

Physical Plane

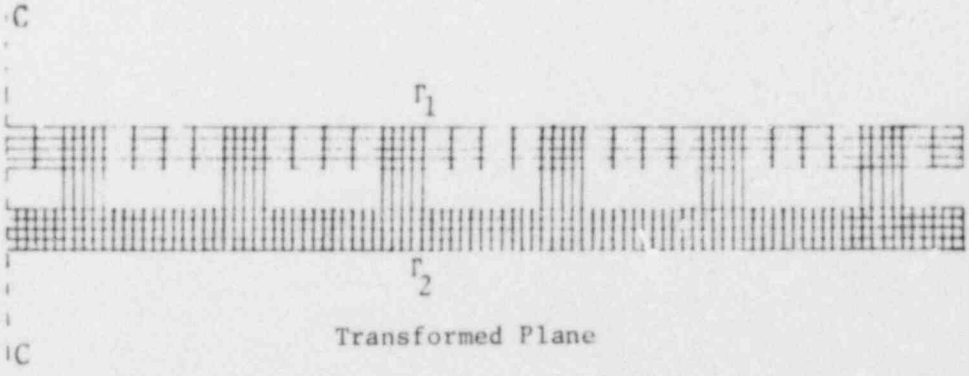

Transformed Plane

Fig. 5. Physical and Transformed Coordinate Systems

Accurate representation of boundary conditions is best accomplished when the boundary is coincident with a coordinate line, so that the boundary can be made to pass through the points of a finite difference grid constructed on the coordinate lines. Finite difference expressions at or adjacent to the boundary may then be applied, using only grid points on the intersections of coordinate lines. Interpolation between grid points is not required, and this is particularly important for boundaries with strong curvature, such as fuel rods.

In the Navier-Stokes equations, the boundary conditions are the dominant influence on the character of the solution; therefore, the use of grid points that are not coincident with the boundaries places the most inaccurate difference representation in precisely the region of greatest sensitivity. The generation of a curvilinear coordinate system with coordinate lines coincident with all boundaries is thus an important aspect of a general numerical solution of the Navier-Stokes equations.

As mentioned before, applications to the rod bundle or reactor fuel assembly, as shown in Fig. 6, is the primary interest of coordinate transformation. Thus, the transformation is basically two-dimensional. However, the transformation outlined below is very general; it can apply to any boundary shape and can be readily extended to three dimensions (a general treatment of the time-dependent movable boundary problem and the control of coordinate system is discussed in Ref. 19).

1. Mathematical Preliminaries

Two-dimensional elliptic boundary value problems are considered. The general transformation from the physical plane (x, y) to the transformed plane (ξ, η) is

$$\xi = \xi(x, y) \quad ,$$

and

$$\eta = \eta(x, y) \quad ; \tag{39}$$

and the inverse transformation is

$$x = x(\xi, \eta) \quad ,$$

and

$$y = y(\xi, \eta) \quad . \tag{40}$$

The Jacobian of the transformation is

$$J = J\left(\frac{x, y}{\xi, \eta}\right) = x_\xi y_\eta - x_\eta y_\xi \neq 0 \quad , \tag{41}$$

where

$$\xi_x = y_\eta / J, \quad \xi_y = -x_\eta / J, \quad \eta_x = -y_\xi / J, \quad \eta_y = -x_\xi / J \quad , \tag{42}$$

$$f_x = (y_\eta f_\xi - y_\xi f_\eta)/J \quad ,$$

$$f_y = (x_\xi f_\eta - x_\eta f_\xi)/J \quad , \tag{43}$$

$$f_{xx} = (y_\eta^2 f_{\xi\xi} - 2y_\xi y_\eta f_{\xi\eta} + y_\xi^2 f_{\eta\eta})/J^2 + [(y_\eta^2 y_{\xi\xi} - 2y_\xi y_\eta y_{\xi\eta} + y_\xi^2 y_{\eta\eta})$$

$$(x_\eta f_\xi - x_\xi f_\eta) + (y_\eta^2 x_{\xi\xi} - 2y_\xi y_\eta x_{\xi\eta} + y_\xi^2 x_{\eta\eta})(y_\xi f_\eta - y_\eta f_\xi)]/J^3 \quad ,$$

and

$$f_{yy} = (x_\eta^2 f_{\xi\xi} - 2x_\xi x_\eta f_{\xi\eta} + x_\xi^2 f_{\eta\eta})/J^2 + [(x_\eta^2 y_{\xi\xi} - 2x_\xi x_\eta y_{\xi\eta} + x_\xi^2 y_{\eta\eta})$$

$$(x_\eta f_\xi - x_\xi f_\eta) + (x_\eta^2 x_{\xi\xi} - 2x_\xi x_\eta x_{\xi\eta} + x_\xi^2 x_{\eta\eta})(y_\xi f_\eta - y_\eta f_\xi)]/J^3 \quad , \tag{44}$$

Higher derivatives can be obtained by repeating the above operations.

Two tasks are involved in the transformation: one is to find the interior physical points after specifying the physical boundary at a number of discrete points. The other is to transform the partial differential equations of interest into the new variables before being approximated by the finite-difference equations.

2. Mapping of Physical Domain [19]

The choice of this mapping is largely dependent on its simplicity and effort required for a desired accuracy. Without loss of generality, a simply connected region will be considered first, and a doubly connected region will be discussed in subsequent sections.

a. Simply Connected Region

The boundary of the physical domain (x ,y) is specified at discrete points corresponding to boundary points in the transformed plane (ξ, η). It is desirable to have a prescribed, convenient mesh in the (ξ, η) plane; therefore, (ξ, η) must be used as independent variables. Their values are governed by any suitable elliptic partial differential equations as a boundary value problem. The simplest choice appears to be that ξ, η must satisfy the Laplace equation in the physical plane:

$$\nabla^2 \xi = 0 \quad , \tag{45}$$

$$\nabla^2 \eta = 0 \quad , \tag{46}$$

where

$$\nabla^2 = \frac{\partial^2}{\partial x^2} + \frac{\partial^2}{\partial y^2} \quad .$$

The dependent and independent variables can be interchanged by applying Eqs. (42) - (44). The transformed equations are:

$$\alpha x_{\xi\xi} - 2\beta x_{\xi\eta} + \gamma x_{\eta\eta} = 0 \quad , \tag{47}$$

and

$$\alpha y_{\xi\xi} - 2\beta y_{\xi\eta} + \gamma y_{\eta\eta} = 0 \quad , \tag{48}$$

where

$$\alpha = x_\xi^2 + y_\xi^2 \quad , \quad \beta = x_\xi x_\eta + y_\xi y_\eta \quad , \quad \gamma = x_\eta^2 + y_\eta^2 \quad . \tag{49}$$

Equations (47) and (48) are clearly coupled quasi-linear elliptic equations, and only in special cases ($x_\xi = y_\eta$ and $x_\eta = y_\xi$) can they be reduced to Laplace equations for which mapping is conformal.

Equations (47) and (48) can be conveniently solved by the finite-difference method, using second-order central differences with successive over-relaxation (SOR) of the dependent variables. Discrete values of (x, y) at the corresponding point (ξ, η) are thus determined.

In general, the numerically calculated boundary may not coincide completely with the given boundary at intermediate points. This is not an essential limitation since only discrete points are needed in the basic principle of the finite difference method. The finer the mesh, the smaller the numerical error.

b. Doubly Connected Region

Consider the transformation of a two-dimensional, doubly connected region D bounded by two simple, closed, arbitrary contours onto a rectangular region D^* as shown in Fig. 6. The basic transformation is discussed here, assuming that the body contour and outer boundary are transformed, respectively, to the constant η-lines forming the bottom and top sides of the transformed region. The more general case of segmented body contours transforming to any side of the transformed region follows analogously. Let Γ_1 map onto Γ_1^*, Γ_2 map onto Γ_2^*, Γ_3 onto Γ_3^*, and Γ_4 onto Γ_4^*. For identification purposes, region D will be referred to as the physical plane, D^* as the transformed plane, and Γ_1 and Γ_2 as the body contours. Note that the transformed boundaries (Γ_1^* and Γ_2^*) are made constant coordinate lines (η-lines) in the transformed plane. The contours Γ_3 and Γ_4, which connect the contours Γ_1 and Γ_2, are coincident in the physical plane and thus constitute re-entrant boundaries in the transformed plane.

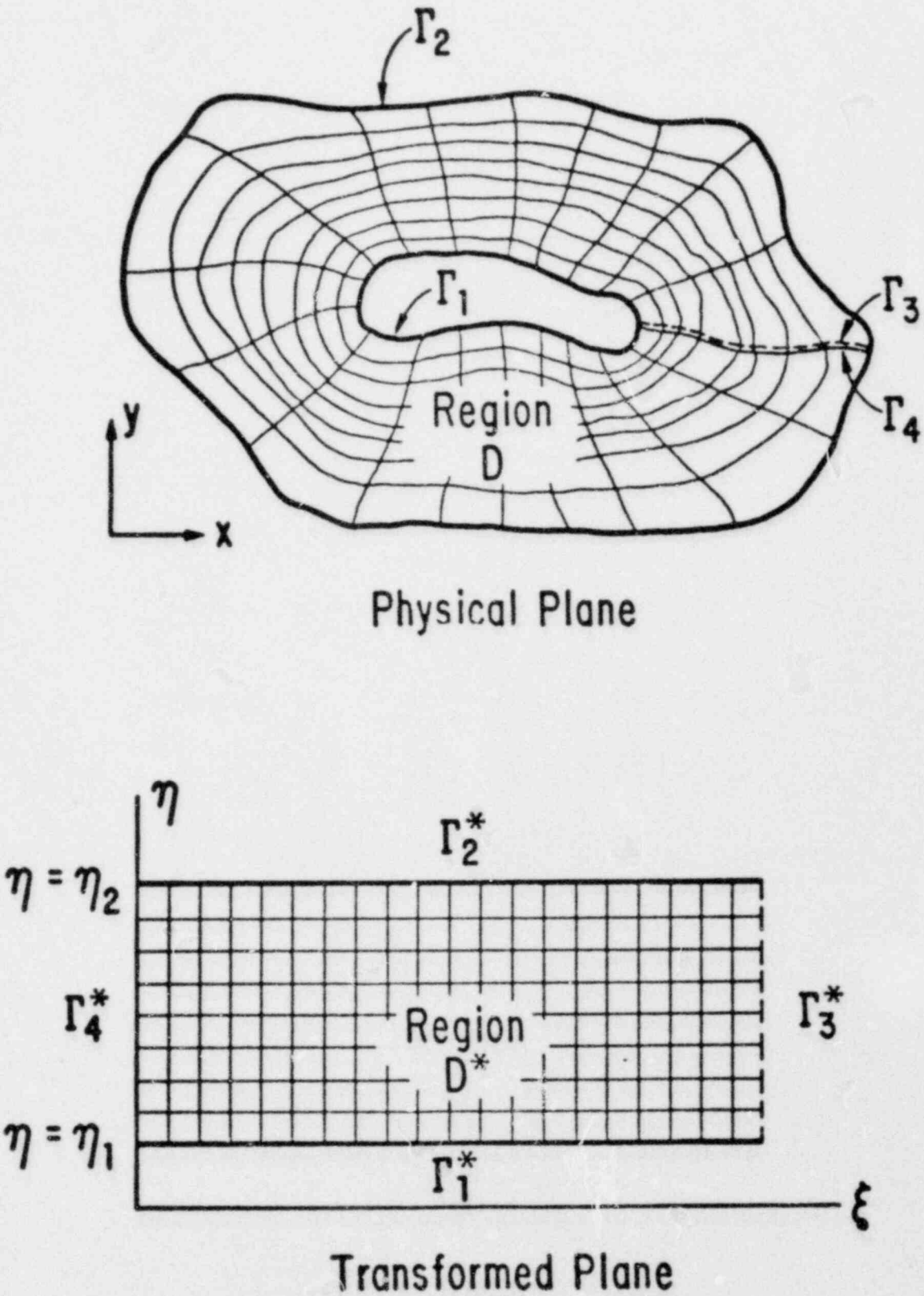

Fig. 6. Field Transformation: Single Body

Let $\xi(x, y)$ and $\eta(x, y)$ be continuous function in D, then

$$\nabla^2 \xi = 0 \quad , \tag{50}$$

$$\nabla^2 \eta = 0 \quad , \tag{51}$$

with the Dirichlet boundary conditions

$$\begin{bmatrix} \xi \\ \\ \eta \end{bmatrix} = \begin{bmatrix} \xi_1(x, y) \\ \\ \eta_1 \end{bmatrix} \quad , \quad [x, y] \in \Gamma_1 \tag{52}$$

$$\begin{bmatrix} \xi \\ \\ \eta \end{bmatrix} = \begin{bmatrix} \xi_2(x, y) \\ \\ \eta_2 \end{bmatrix} \quad , \quad [x, y] \in \Gamma_2 \tag{53}$$

where η_1 and η_2 are different constants $(\eta_2 > \eta_1)$, and $\xi_1(x, y)$ and $\xi_2(x, y)$ are specified monotonic functions on Γ_1 and Γ_2, respectively, varying over the same range. The arbitrary curve joining Γ_1 and Γ_2 in the physical plane, which transforms to the right and left sides of the transformed plane, specifies a branch cut for the multiple-valued function $\xi(x, y)$. Thus, the values of the physical coordinate functions $x(\xi, \eta)$ and $y(\xi, \eta)$ are the same on Γ_3 as on Γ_4, and these functions and their derivatives are continuous from Γ_3 to Γ_4. Therefore, boundary conditions are neither required nor allowed on Γ_3 and Γ_4.

Since it is desired to perform all numerical computations in the uniform rectangular transformed plane, the dependent and independent variables must be interchanged in Eqs. (50) and (51), similar to Eqs. (47) and (48):

$$\alpha x_{\xi\xi} - 2\beta x_{\xi\eta} + \gamma x_{\eta\eta} = 0 \quad , \tag{54}$$

and

$$\alpha y_{\xi\xi} - 2\beta y_{\xi\eta} + \gamma y_{\eta\eta} = 0 \quad , \tag{55}$$

where α, β, and γ are defined as before, with the transformed boundary conditions

$$\begin{bmatrix} x \\ \\ y \end{bmatrix} = \begin{bmatrix} f_1(\xi, \eta_1) \\ \\ f_2(\xi, \eta_1) \end{bmatrix} \quad , \quad [\xi, \eta_1] \in \Gamma_1^* \tag{56}$$

$$\begin{bmatrix} x \\ \\ y \end{bmatrix} = \begin{bmatrix} g_1(\xi, \eta_2) \\ \\ g_2(\xi, \eta_2) \end{bmatrix} \quad , \quad [\xi, \eta_2] \in \Gamma_2^* \tag{57}$$

The functions $f_1(\xi, \eta_1)$, $f_2(\xi, \eta_1)$, $g_1(\xi, \eta_2)$, and $g_2(\xi, \eta_2)$ are specified by the known shape of the contours Γ_1 and Γ_2 and the specified distribution of ξ thereon. As noted, boundary conditions are neither required nor allowed along the re-entrant boundaries Γ_3^* and Γ_4^*.

The system given by Eqs. (54) and (55) is a quasi-linear elliptic system for the physical coordinate functions $x(\xi, \eta)$ and $y(\xi, \eta)$ in the transformed plane. As pointed out before, although this system is considerably more complex than that given by Eqs. (50) and (51), the boundary conditions, Eqs. (56) and (57), are specified on straight boundaries, and the coordinate spacing in the transformed plane is uniform. The boundary fitted coordinate system generated by the solution of Eqs. (54) - (57) has a constant η-line coincident with each boundary in the physical plane. The ξ-constant lines may be spaced as desired around the boundaries since the assignment of the ξ-values to the [x, y] boundary points via the functions f_1, f_2, g_1, and g_2 in Eqs. (56) and (57) is arbitrary. Numerically, the discrete boundary values [x, y] are transformed to equally spaced discrete ξ_k-points on both boundaries. As illustrated in Fig. 6, the left and right boundaries of the transformed plane are re-entrant boundaries, which imply that both solutions, $x(\xi, \eta)$ and $y(\xi, \eta)$, are required to be periodic in the region $\{[\xi, \eta] \mid -\infty < \xi < \infty, \eta_1 \leq \eta \leq \eta_2\}$.

The analogous cylindrical coordinates used in the work [16] fall into the category of this section. In this case, the fuel assembly center line plays the role of the curve Γ_1 in Fig. 6. This curve is thus collapsed to a point. Extension to a multiply connected region is straightforward.

3. Preservation of Equation Type

When coordinate transformations are utilized as an aid in solving a given partial differential equation, it is imperative that the equation not change type under the transformation. Such an invariance will now be demonstrated for the transformation of the system equations of interest. Consider the general, second order quasi-linear partial differential equation

$$A(x, y, f)f_{xx} + B(x, y, f)f_{xy} + C(x, y, f)f_{yy} + E(x, y, f)f_x + F(x, y, f)f_y + G(x, y, f) = 0 \quad , \tag{58}$$

where $F = f(x, y)$ is a twice continuously differentiable scalar function, and A, B, C, E, F, and G are continuous functions. Recall that the equation type is determined by the coefficient functions A, B, and C as follows:

Elliptic if $B^2 - 4AC < 0$,

Parabolic if $B^2 - 4AC = 0$,

and

Hyperbolic if $B^2 - 4AC > 0$.

It can readily be shown that Eq. (58) transforms to

$$A^* f_{\xi\xi} + B^* f_{\xi\eta} + C^* f_{\eta\eta} + E^* f_{\xi} + F^* f_{\eta} + G^* = 0 \quad , \tag{59}$$

where

$$A^* \equiv A\xi_x^2 + B\xi_x\xi_y + C\xi_y^2 \quad ,$$

$$B^* \equiv 2A\xi_x\eta_x + B(\xi_x\eta_y + \xi_y\eta_x) + 2C\xi_y\eta_y \quad ,$$

$$C^* \equiv A\eta_x^2 + B\eta_x\eta_y + C\eta_y^2 \quad ,$$

$$E^* \equiv 2A\xi_{xx} + B\xi_{xy} + C\xi_{yy} + E\xi_x + F\xi_y \quad ,$$

$$F^* \equiv A\eta_{xx} + B\eta_{xy} + C\eta_{yy} + E\eta_x + F\eta_y \quad ,$$

and

$$F^* \equiv F \quad .$$

Now, consider $(B^*)^2 - 4A^*C^*$:

$$(B^*)^2 - 4A^*C^* = [2A\xi_x\eta_x + B(\xi_x\eta_y + \eta_x\xi_y) + 2C\xi_y\eta_y]^2$$

$$- 4(A\xi_x^2 + B\xi_x\xi_y + C\xi_y^2)(A\eta_x^2 + B\eta_x\eta_y + C\eta_y^2)$$

$$= (B^2 + 4AC)(\xi_x\eta_y - \xi_y\eta_x)^2$$

$$= (B^2 - 4AC)/J^2 \quad .$$

Since $J^2 > 0$, $B^2 - 4AC$ and $(B^*)^2 - 4A^*C^*$ are either both positive, both negative, or both zero. This implies that Eqs. (58) and (59) are of the same type.

4. Governing Equations in Non-Dimensional Form

$$\frac{\partial \rho}{\partial t} + \frac{\partial (\rho u_j)}{\partial x_j} = 0 \quad , \tag{60}$$

$$\frac{\partial (\rho u_i)}{\partial t} + \frac{\partial (\rho u_i u_j)}{\partial x_j} = \frac{\partial \tau_{ij}}{\partial x_j} - \rho g_j \quad , \tag{61}$$

and

$$\frac{\partial E}{\partial t} + \frac{\partial (u_j E)}{\partial x_j} = D \frac{\partial (u_i \tau_{ij})}{\partial x_j} - \frac{\partial q_j}{\partial x_j} + \dot{Q} \quad , \tag{62}$$

The variables in the conservation equations are non-dimensionalized with respect to the reference velocity (V_o), length (L_o), density (ρ_o), enthalpy (h_o), gravitational constant (g_o), viscosity (μ_o), thermal conductivity (κ_o), and specific heat (c_{po}), as follows:

$$(u_i)_{ND} = \frac{u_i}{V_o} \quad ,$$

$$(t)_{ND} = \frac{t}{(L_o/V_o)} \quad ,$$

$$(\rho)_{ND} = \frac{\rho}{\rho_o} \quad ,$$

$$(x_i)_{ND} = \frac{x_i}{L_o} \quad ,$$

$$(E)_{ND} = \frac{E}{\rho_o h_o} \quad ,$$

$$(g)_{ND} = \frac{g}{g_o} \quad ,$$

$$(e)_{ND} = \frac{e}{h_o} \quad ,$$

$$(p)_{ND} = \frac{p}{\rho_o h_o} \quad ,$$

$$(T)_{ND} = \frac{T}{(g_o/C_{po})} \quad ,$$

$$(\mu)_{ND} = \frac{\mu}{\mu_o} \quad ,$$

$$(\kappa)_{ND} = \frac{\kappa}{\kappa_o} \quad ,$$

$$(\tau_{ij})_{ND} = \frac{\tau_{ij}}{\rho_o h_o} \quad ,$$

$$(q_i)_{ND} = \frac{q_i}{\rho_o h_o V_o} \quad ,$$

and

$$(\dot{Q})_{ND} = \frac{\dot{Q}}{(h_o \rho_o V_o / L_o)} \quad ,$$

where subscript ND denotes non-dimensional and is deleted in Eqs. (60) - (62) for simplicity, and

$$E = \rho\left(e + D\,\frac{u^2}{2}\right) = \rho\left(h + D\,\frac{u^2}{2}\right) - p \quad ,$$

$$\tau_{ij} = -\frac{1}{D}\,p\delta_{ij} + \frac{1}{R}\,\mu\left(\frac{\partial u_i}{\partial x_j} + \frac{\partial u_j}{\partial x_i}\right) \quad ,$$

and

$$q_i = -\frac{1}{RP}\,\kappa\,\frac{\partial T}{\partial x_i} \quad ,$$

with the non-dimensional numbers

$$R = \frac{V_o L_o \rho_o}{\mu_o} = \text{Reynolds number} \quad ,$$

$$P = \frac{\mu_o C_{po}}{\kappa_o} = \text{Prandtl number} \quad ,$$

and

$$D = \frac{V_o^2}{h_o} \quad .$$

5. Transformed Governing Equations

The boundary fitted curvilinear coordinates are taken such that ξ and η lie in the plane normal to the fuel assembly axis, with ζ parallel to this axis. The planes are assumed equally spaced along the axis so that, with Z along the axis,

$$Z_\zeta \equiv \frac{dZ}{d\zeta} = \text{Constant} \quad . \tag{63}$$

The Cartesian coordinates x and y lie in the plane normal to the fuel assembly axis.

After transformation to the ξ, η, ζ system, the governing equations in non-dimensional form become:

$$\frac{\partial \rho}{\partial t} + \frac{1}{J}\frac{\partial(\rho\hat{u})}{\partial \xi} + \frac{1}{J}\frac{\partial(\rho\hat{v})}{\partial \eta} + \frac{d\zeta}{dZ}\frac{\partial(\rho w)}{\partial \zeta} = 0 \quad , \tag{64}$$

$$\frac{\partial(\rho u)}{\partial t} + \frac{1}{J}\frac{\partial(\rho u\hat{u})}{\partial \xi} + \frac{1}{J}\frac{\partial(\rho u\hat{v})}{\partial \eta} + \frac{d\zeta}{dZ}\frac{\partial(\rho uw)}{\partial \zeta}$$

$$= \frac{1}{J}\frac{\partial}{\partial \xi}\left(y_\eta \tau_{11} - x_\eta \tau_{21}\right) + \frac{1}{J}\frac{\partial}{\partial \eta}\left(x_\xi \tau_{21} - y_\xi \tau_{11}\right) + \frac{d\zeta}{dZ}\frac{\partial(\tau_{31})}{\partial \zeta} \quad , \tag{65}$$

$$\frac{\partial(\rho v)}{\partial t} + \frac{1}{J}\frac{\partial(\rho v\hat{u})}{\partial \xi} + \frac{1}{J}\frac{\partial(\rho v\hat{v})}{\partial \eta} + \frac{d\zeta}{dZ}\frac{\partial(\rho vw)}{\partial \zeta}$$

$$= \frac{1}{J}\frac{\partial}{\partial \xi}\left(y_\eta \tau_{12} - x_\eta \tau_{22}\right) + \frac{1}{J}\frac{\partial}{\partial \eta}\left(x_\xi \tau_{22} - y_\xi \tau_{12}\right) + \frac{d\zeta}{dZ}\frac{\partial(\tau_{12})}{\partial} \quad , \tag{65a}$$

$$\frac{\partial(\rho w)}{\partial t} + \frac{1}{J}\frac{\partial(\rho w\hat{u})}{\partial \xi} + \frac{1}{J}\frac{\partial(\rho w\hat{v})}{\partial \eta} + \frac{d\zeta}{dZ}\frac{\partial(\rho ww)}{\partial \zeta}$$

$$= \frac{1}{J}\frac{\partial}{\partial \xi}\left(y_\eta \tau_{13} - x_\eta \tau_{23}\right) + \frac{1}{J}\frac{\partial}{\partial \eta}\left(x_\xi \tau_{23} - y_\xi \tau_{13}\right) + \frac{d\zeta}{dZ}\frac{\partial(\tau_{33})}{\partial \zeta} - \rho g \quad , \tag{65b}$$

and

$$\frac{\partial E}{\partial t} + \frac{1}{J}\frac{\partial(\hat{Eu})}{\partial \xi} + \frac{1}{J}\frac{\partial(\hat{Ev})}{\partial \eta} + \frac{d\zeta}{dZ}\frac{\partial(Ew)}{\partial \zeta}$$

$$= -\frac{1}{J}\frac{\partial(\hat{pu})}{\partial \xi} - \frac{1}{J}\frac{\partial(\hat{pv})}{\partial \eta} + \frac{d\zeta}{dZ}\frac{\partial(pw)}{\partial \zeta}$$

$$+ \frac{D}{J}\frac{\partial}{\partial \xi}\left[y_\eta(\tau_{11}u + \tau_{12}v + \tau_{13}w) - x_\eta(\tau_{21}u + \tau_{22}v + \tau_{23}w)\right]$$

$$+ \frac{D}{J}\frac{\partial}{\partial \eta}\left[x_\xi(\tau_{21}u + \tau_{22}v + \tau_{23}w) - y_\xi(\tau_{11}u + \tau_{12}v + \tau_{13}w)\right]$$

$$+ D\frac{d\zeta}{dZ}\frac{\partial}{\partial \zeta}(\tau_{31}u + \tau_{32}v + \tau_{33}w)$$

$$+ \frac{1}{JRP}\frac{\partial}{\partial \zeta}(y_\eta \kappa T_x - x_\eta \kappa T_y) + \frac{1}{JRP}\frac{\partial}{\partial \eta}(x_\xi \kappa T_y - y_\xi \kappa T_x)$$

$$+ \frac{1}{RP}\frac{d\zeta}{dZ}\frac{\partial}{\partial \zeta}(\kappa T_z) + \dot{Q} \quad . \tag{66}$$

The stress terms in the momentum equations are

$$y_\eta \tau_{11} - x_\eta \tau_{21} = -\frac{1}{D} C_8 p + \frac{\mu}{R}\left(C_9 u_\xi - C_{13} u_\eta - C_{16} v_\xi + C_{18} v_\eta - \frac{2}{3} C_8 \frac{d\zeta}{dZ} w_\zeta\right) ,$$

$$x_\xi \tau_{21} - y_\xi \tau_{11} = -\frac{1}{D} C_7 p + \frac{\mu}{R}\left(C_{13} u_\xi - C_{11} u_\eta - C_{17} v_\xi + C_{15} v_\eta - \frac{2}{3} C_7 \frac{d\zeta}{dZ} w_\zeta\right) ,$$

$$\tau_{31} = \frac{\mu}{R}\left[\frac{d\zeta}{dZ} u_z + 2 C_1(C_8 w_\xi - C_7 w_\eta)\right] ,$$

$$y_\eta \tau_{12} - x_\eta \tau_{22} = -\frac{1}{D} C_6 p + \frac{\mu}{R}\left(C_{16} u_\xi - C_{17} u_\eta - C_{10} v_\xi + C_{14} v_\eta - \frac{2}{3} C_6 \frac{d\zeta}{dZ} w_\zeta\right) ,$$

$$x_\xi \tau_{22} - y_\xi \tau_{12} = -\frac{1}{D} C_5 p + \frac{\mu}{R}\left(C_{18} u_\xi - C_{15} u_\eta - C_{14} v_\xi + C_{12} v_\eta - \frac{2}{3} C_5 \frac{d\zeta}{dZ} w_\zeta\right) ,$$

$$\tau_{32} = \frac{\mu}{R}\left[\frac{d\zeta}{dZ} v_z + 2 C_1(C_5 w_\eta - C_6 w_\xi)\right] ,$$

$$y_\eta \tau_{13} - x_\eta \tau_{23} = \frac{\mu}{R}\left[C_2 w_\xi - C_3 w_\eta + \frac{d\zeta}{dZ}\left(C_8 u_\zeta - C_6 v_\zeta\right)\right] \quad ,$$

$$x_\xi \tau_{23} - y_\xi \tau_{13} = \frac{\mu}{R}\left[C_4 w_\eta - C_3 w_\xi + \frac{d\zeta}{dZ}\left(C_5 u_\zeta - C_7 v_\zeta\right)\right] \quad ,$$

and

$$\tau_{33} = -\frac{1}{D} p + \frac{\mu}{R}\left[\frac{4}{3}\frac{d\zeta}{dZ} w_\zeta - \frac{2}{3}(2C_1)(C_8 u_\xi - C_7 u_\eta + C_5 v_\eta - C_6 v_\xi)\right] \quad .$$

The stress terms in the energy equation are:

$$y_\eta(\tau_{11}u + \tau_{12}v + \tau_{13}w) - x_\eta(\tau_{21}u - \tau_{22}v + \tau_{23}w)$$

$$= \frac{\mu}{R}\left[(C_9 u - C_{16} v)u_\xi + (C_{17} v - C_{13} u)u_\eta + C_8 w \frac{d\zeta}{dZ} u_\zeta\right.$$

$$+ (C_{10} v - C_{16} u)v_\xi + (C_{18} u - C_{14} v)v_\eta - C_6 w \frac{d\zeta}{dZ} v_\zeta$$

$$\left. + C_2 w w_\xi - C_3 w w_\eta - \frac{2}{3}\hat{u}\frac{d\zeta}{dZ} w_\zeta\right] \quad ,$$

$$x_\xi(\tau_{21}u + \tau_{22}v + \tau_{23}w) - y_\xi(\tau_{11}u - \tau_{12}v + \tau_{13}w)$$

$$= \frac{\mu}{R}\left[(C_{18} v - C_{13} u)u_\xi + (C_{11} u - C_{15} v)u_\eta - C_7 w \frac{d\zeta}{dZ} u_\zeta\right.$$

$$+ (C_{17} u - C_{14} v)v_\xi + (C_{12} v - C_{15} u)v_\eta + C_5 w \frac{d\zeta}{dZ} v_\zeta$$

$$\left. + C_4 w w_\eta - C_3 w w_\xi - \frac{2}{3}\hat{v}\frac{d\zeta}{dZ} w_\zeta\right] \quad ,$$

and

$$\tau_{31}u + \tau_{32}v + \tau_{33}w = \frac{\mu}{R}\left(-\frac{4}{3} C_1 C_8 w u_\xi + \frac{4}{3} C_1 C_7 w u_\eta + u \frac{d\zeta}{dZ} u_\zeta\right.$$

$$+ \frac{4}{3} C_1 C_6 w v_\xi - \frac{4}{3} C_1 C_7 w v_\eta + v \frac{d\zeta}{dZ} v_\zeta$$

$$+ 2C_1 \hat{u} w_\xi + 2C_1 \hat{v} w_\eta + \frac{4}{3} w \frac{d\zeta}{dZ} w_\zeta \Big) \quad .$$

The conduction terms are:

$$\kappa(y_\eta T_x - x_\eta T_y) = \kappa(C_2 T_\xi - C_3 T_\eta) \quad ,$$

$$\kappa(x_\xi T_y - y_\xi T_x) = \kappa(C_4 T_\eta - C_3 T_\xi) \quad ,$$

and

$$\kappa T_z = \kappa \frac{d\zeta}{dZ} T_\zeta \quad .$$

The coefficients in these relations are defined

$$C_1 \equiv \frac{1}{2J} \quad , \qquad C_{10} \equiv \frac{1}{3J}(3\alpha + x_\eta^2) \quad ,$$

$$C_2 \equiv \frac{\alpha}{J} \quad , \qquad C_{11} \equiv \frac{1}{3J}(3\gamma + y_\xi^2) \quad ,$$

$$C_3 \equiv \frac{\beta}{J} \quad , \qquad C_{12} \equiv \frac{1}{3J}(3\gamma + x_\xi^2) \quad ,$$

$$C_4 \equiv \frac{\gamma}{J} \quad , \qquad C_{13} \equiv \frac{1}{3J}(3\beta + y_\xi y_\eta) \quad ,$$

$$C_5 \equiv x_\xi \quad , \qquad C_{14} \equiv \frac{1}{3J}(3\beta + x_\xi x_\eta) \quad ,$$

$$C_6 \equiv x_\eta \quad , \qquad C_{15} \equiv \frac{x_\xi y_\xi}{3J} \quad ,$$

$$C_7 \equiv y_\xi \quad , \qquad C_{16} \equiv \frac{x_\eta y_\eta}{3J} \quad ,$$

$$C_7 \equiv y_\xi \quad , \qquad C_{16} \equiv \frac{x_\eta y_\eta}{3J} \quad ,$$

$$C_8 \equiv y_\eta \quad , \qquad C_{17} \equiv \frac{1}{3J}\left(x_\eta y_\xi + 2J\right) \quad ,$$

$$C_9 \equiv \frac{1}{3J}\left(3\alpha + y_\eta^2\right) \quad , \qquad C_{18} \equiv \frac{1}{3J}\left(x_\eta y_\xi - 2J\right) \quad ,$$

with

$$J = x_\xi y_\eta - x_\eta y_\xi \quad , \qquad \hat{u} = uy_\eta - vx_\eta \quad ,$$

$$\alpha = x_\eta^2 + y_\eta^2 \quad , \qquad \hat{v} = vx_\xi - uy_\xi \quad ,$$

$$\beta = x_\xi x_\eta + y_\xi y_\eta \quad , \qquad \gamma = x_\xi^2 + y_\xi^2 \quad .$$

6. Initial and Boundary Conditions and Numerical Technique

The initial and boundary conditions and numerical technique employed in the benchmark rod-bundle thermal-hydraulic analysis are similar to those used in the porous medium formulation with volume porosity, surface permeability, distributed resistance, and distributed heat source outlined in the previous section, except that the modified staggered mesh system is used in which pressure, density, temperature or enthalpy are specified at cell center, and all velocities are specified at the intersections of grid lines. Some recent numerical results obtained from BODYFIT-1 are presented in the paper by Chen, Vanka, and Sha [18].

III. CONCLUSION

Three pertinent methods used in rod-bundle thermal-hydraulic analysis are presented. These methods are (1) subchannel analysis, (2) porous medium formulation, and (3) benchmark rod-bundle thermal-hydraulic analysis using a boundary fitted coordinate system. Basic limitations of methods (1) and (2) are clearly delineated. In subchannel analysis, the transverse momentum equation cannot be treated with the same rigor as the axial momentum equations, due to subchannel arrangement. The usual justification of neglecting the diffusion term in momentum equations is that drag due to the presence of rods is much larger than viscous diffusion. This assumption is no longer valid when recirculatory flow is encountered, such as in the analysis of flow blockage. Furthermore, approximations must be employed for simplification of geometrical configuration of the control volume for the transverse momentum equation and interfacing information between two different control volumes, e.g., one for the transverse momentum equation, and another for the axial momentum equation. These basic limitations are inherent; therefore, validity

of subchannel analysis to situations with large flow disturbance poses serious concern. The porous medium formulation with volume porosity, surface permeability, distributed resistance and distributed heat source is used in the COMMIX code, and it eliminates some of the limitations employed in subchannel analysis. The concept of surface permeability is new in porous medium formulation, and it greatly facilitates characterization of an anisotropic medium. In general, it improves accuracy of results since surface permeability is well defined and distributed resistance is not precisely known in most engineering applications. Furthermore, the porous medium formulation provides a greater range of applicability. As an example, the COMMIX code is capable of treating both continuum (reactor plenum mixing, piping analysis, etc.) and quasi-continuum (fuel assembly, heat exchangers, etc.) problems. This capability represents a very cost-effective way of developing a computer code.

However, accurate determination of distributed resistance in a complex rod-bundle geometry requires fine structure of both temperature and velocity. The most rigorous rod-bundle thermal-hydraulic analysis uses a boundary fitted coordinate transformation. Each rod is explicitly represented as an internal boundary; thus, appropriate boundary conditions can be specified. After the coordinate transformation, the complex rod-bundle geometry reduces to a multiply connected continuum in a rectangular region with all boundaries coincident with the grid lines. However, the system of equations to be solved in the transformed plane is more complicated than the original one. Most important of all, the empirical mixing coefficients and cross flow resistances normally associated with a rod-bundle thermal-hydraulic analysis are eliminated, thereby enhancing computational stability and accuracy. As a matter of fact, for laminar flow, this method gives solutions without any assumptions, and it requires information only on rod bundle geometry and thermal physical properties of the fluid; for turbulent flow, empiricism is needed due to the enclosure problem encountered in turbulence modeling. However, one drawback of benchmark rod-bundle thermal-hydraulic analysis using a boundary fitted coordinate system is that it requires large computer storage and long running time, and thus, is limited to relatively small rod-bundle sizes or a local region of interest in a large rod bundle.

Recently, the effect of distorted geometry on thermal-hydraulic performance in a fuel assembly has received a great deal of attention. Once the fuel elements are distorted (in an arbitrary way), the geometrical flow paths become very complex, making their accurate representation in conventional simulation very difficult. The difficulties encountered in subchannel analyses are the following:

a. The subchannel representations with an arbitrarily distorted configuration in a rod bundle are very difficult, especially in the axial direction.

b. Because of the distortion, the mixing coefficients, hydraulic resistances, and conduction lengths used in the flow and heat transfer calculations need to be recalibrated. This is a difficult task for various distorted configurations. This difficulty is further compounded by the inherent approximations used in the transverse momentum equations.

c. The fuel rod boundaries are inclined with the normals to the subchannel, and the velocities are at an angle with the fuel rods. Because the finite-difference grid does not align with the boundaries, representation of the boundary conditions will be difficult and inaccurate.

Therefore, subchannel analysis for distorted rod bundle geometries can be subject to significant difficulties and error. The porous medium approach has the advantage over subchannel analysis in that the distorted geometry can be represented more conveniently and accurately by varying the volume porosity and surface permeability. It also removes the inherent assumptions used in the transverse momentum equations associated with subchannel analysis. The advantage of using correct transverse momentum equations is significant when the flow is not dominant in the axial direction. It should be noted that empirical calibration of the distributed resistance with experimental data corresponding to the distorted geometry is necessary. The distributed resistance of a given distorted configuration may be estimated by using the benchmark rod-bundle thermal-hydraulic analysis with the three-dimensional boundary fitted coordinate transformation. The combined use of the porous medium formulation (COMMIX code) and benchmark rod-bundle thermal-hydraulic analysis using boundary fitted coordinate system (BODYFIT code) represents one of the most sound and cost effective approaches to the distorted geometry problem. In summary, the proposed approach using the COMMIX and BODYFIT codes can greatly reduce the required experimental data base for representing unlimited possibilities of distorted geometry.

ACKNOWLEDGEMENTS

The author is indebted to Professors B. T. Chao, J. C. Slattery, and S. L. Soo for stimulating discussions on the quasi-continuum formulation; to Professor J. F. Thompson for his contribution on benchmark rod-bundle thermal-hydraulic analysis; to my co-workers Drs. H. M. Domanus, V. L. Shah, B. C. Chen, S. P. Vanka, and R. C. Schmitt for their general support; to Mrs. S. A. Moll for her excellent typing of this paper, and most, importantly, to Drs. R. T. Curtis, C. N. Kelber, and Mr. P. M. Wood of the United States Nuclear Regulatory Commission (Contract No. A2045) for their support of this work, and to Drs. B. R. Sehgal and J. Kim of the Electric Power Research Institute (Contract No. 1383-1) for his partial support of the BODYFIT code development and application efforts.

REFERENCES

1. W. T. Sha and R. C. Schmitt, *THI3D: A Computer Program for Steady-State Thermal-Hydraulic Multichannel Analysis*, ANL-8112 (Dec 1975); also see W. T. Sha, R. C. Schmitt, and E. I. H. Lin, *THI3D-1: A Computer Program for Steady-State Thermal-Hydraulic Multichannel Analysis*, ANL-77-15 (July 1977).

2. D. S. Rowe, *COBRA-IIIC: A Digital Computer Program for Steady-State and Transient Thermal-Hydraulic Analysis of Rod Bundle Nuclear Fuel Elements*, BNWL-1695 (Mar 1973).

   C. W. Stewart et al, *COBRA-IV: The Model and the Method*, BNWL-2214 (1978).

3. R. Potter et al., *SABRE 1: A Computer Program for the Calculation of Three-Dimensional Flows in Rod Clusters*, AEEW-R 1057 (July 1976).

4. W. T. Sha and B. T. Chao, *Conservation Equations for Finite Control Volume Containing Single-Phase Fluid with Fixed, Dispersed Heat Generating (Absorbing) Solids*, NUREG-CR-0945, ANL-CT-79-42 (July 1979).

5. John C. Slattery, *Momentum Energy and Mass Transfer in Continua*, Ch. 4, McGraw-Hill (1972).

6. W. J. Wnek et al., *Transient Three-Dimensional Thermal-Hydraulic Analysis of Nuclear Reactor Fuel Rod Arrays: General Equations and Numerical Scheme*, ANCR-1207 (Nov 1975).

7. W. T. Sha, H. M. Domanus, R. C. Schmitt, J. J. Oras, and E. I. H. Lin, *COMMIX-1: A Three-Dimensional, Transient, Single-Phase Component Computer Program for Thermal-Hydraulic Analysis*, NUREG-0415, ANL-77-96 (Jan 1978).

8. John C. Slattery, *Flow of Viscoelastic Fluids through Porous Media*, AIChE Journal, 13, 6, pp. 1066-107 (1967).

9. J. C. Slattery, *Interfacial Transport Phenomena*, Manuscript of a forthcoming book to be published, Northwestern University, Evanston, Illinois (1981).

10. S. Whitaker, *The Equations of Motion in Porous Media*, Chem. Engrg. Sci., 21, pp. 291- (1966).

11. S. Whitaker, *Diffusion and Dispersion in Porous Media*, AIChE Journal, 13, pp. 420- (1967).

12. William T. Sha and B. T. Chao, *Local Volume Average Transport Equations in Regions Containing Single-Phase Fluid with Dispersed and Stationary Heat Generating Solids*, ANL- (to be published).

13. S. Whitaker, *Introduction to Fluid Mechanics*, Prentice-Hall, Englewood Cliffs (1968).

14. S. Whitaker, *Advances in Theory of Fluid Motion in Porous Media*, Ind. Engrg. Chem., 61, 12, pp. 14-28 (1969).

15. W. T. Sha and C. F. Bonilla, Editors: *A Special Issue on Liquid Metal Fast Breeder Reactor (LMFBR) Single-Phase Rod-Bundle Thermal-Hydraulics*, Nuclear Engineering and Design, to be published (1981).

16. W. T. Sha and J. F. Thompson, *Rod-Bundle Thermal-Hydraulic Analysis using Boundary Fitted Coordinate System*, NUREG-CR-0001, ANL-78-1 (Jan 1978).

17. W. T. Sha, B. C-J. Chen, Y. S. Cha, S. P. Vanka, R. C. Schmitt, J. F. Thompson, and M. L. Doria, *Benchmark Rod-Bundle Thermal-Hydraulic Analysis using Boundary Fitted Coordinates*, ANS Transaction (Nov 1979).

18. B. C-J. Chen, S. P. Vanka, and W. T. Sha, *Some Recent Computations of Rod Bundle Thermal-Hydraulics using Boundary Fitted Coordinates*, in a special issue on Liquid Metal Fast Breeder Reactor (LMFBR) Single-Phase Rod-Bundle Themal-Hydraulics, Nuclear Engineering and Design, to be published (1981).

19. J. F. Thompson, F. C. Thames, and C. W. Mastin, *Boundary-Fitted Curvilinear Coordinate System for Solution of Partial Differential Equations on Fields Containing any Number of Arbitrary Two-Dimensional Bodies - Final Report*, NASA-CR-2729 (1977).

Distribution for NUREG/CR-1825 (ANL-79-10)

Internal:

E. S. Beckjord
C. E. Till
R. S. Zeno
J. G. Bartzis
A. R. Brunsvold
H. M. Domanus
D. M. France
P. Kehler
J. J. Lorenz
C. C. Miao
W. T. Sha (8)
V. L. Shah
M. R. Sims
S. P. Vanka
W. L. Chen
D. H. Cho
M. Ishii
D. R. Ferguson
D. P. Weber
E. M. Gelbard
L. W. Deitrich
R. M. Singer
Y. W. Shin
G. K. Leaf
P. B. Abramson
H. H. Hummel
J. E. Sanecki
ANL Contract File
ANL Libraries (2)
TIS Files (3)

External:

USNRC, for distribution per R7 (380)
DOE-TIC (2)
Manager, Chicago Operations and Regional Office, DOE
Chief, Office of Patent Counsel, DOE-CORO
President, Argonne Universities Association, Argonne, Ill.
Components Technology Division Review Committee:
F. W. Buckman, Consumers Power Co., Jackson, Mich. 49201
P. F. Cunniff, U. Maryland, College Park, Md. 20742
R. A. Greenkorn, Purdue U., West Lafayette, Ind. 47907
W. M. Jacobi, Westinghouse Electric Corp., Pittsburgh, Pa. 15230
M. A. Schultz, North Palm Beach, Fla. 33408
A. Sesonske, Purdue U., West Lafayette, Ind. 47907
J. Weisman, U. Cincinnati, Cincinnati, O. 45221
R. T. Curtis, Div. Reactor Safety Research, USNRC (50)
S. Fabic, Div. Reactor Safety Research, USNRC
S. L. Soo, U. Illinois, Urbana, Ill. 61801
B. T. Chao, U. Illinois, Urbana, Ill. 61801
J. C. Slattery, Northwestern U., Evanston, Ill. 60201
N. E. Todreas, Massachusetts Inst. Technology, Cambridge, Mass. 02139
D. S. Rowe, Rowe and Associates, Bellevue, Wash. 98007
R. Markley, Westinghouse, Advanced Reactor Div., Madison, Pa. 15663
D. S. Trent, Pacific Northwest Lab., Richland, Wash. 99352
A. A. Bishop, U. Pittsburgh, Pittsburgh, Pa. 15261
B. R. Sehgal, Electric Power Research Inst., Palo Alto, Calif. 94303